Axial nucleon and nucleon to Δ form factors and the Goldberger-Treiman relations from lattice QCD

C. Alexandrou,[1] G. Koutsou,[1] Th. Leontiou,[1] J. W. Negele,[2] and A. Tsapalis[3]

[1]*Department of Physics, University of Cyprus, CY-1678 Nicosia, Cyprus*
[2]*Center for Theoretical Physics, Laboratory for Nuclear Science and Department of Physics, Massachusetts Institute of Technology, Cambridge, Massachusetts 02139, USA*
[3]*Institute for Accelerating Systems and Applications, University of Athens, Athens, Greece*

(Received 20 June 2007; published 19 November 2007)

We evaluate the nucleon axial form factor, $G_A(q^2)$, and induced pseudoscalar form factor, $G_p(q^2)$, as well as the pion-nucleon form factor, $G_{\pi NN}(q^2)$, in lattice QCD. We also evaluate the corresponding nucleon to Δ transition form factors, $C_5^A(q^2)$ and $C_6^A(q^2)$, and the pion-nucleon-Δ form factor $G_{\pi N\Delta}(q^2)$. The nucleon form factors are evaluated in the quenched theory and with two degenerate flavors of dynamical Wilson fermions. The nucleon to Δ form factors, besides Wilson fermions, are evaluated using domain wall valence fermions with staggered sea quark configurations for pion masses as low as about 350 MeV. Using these form factors, together with an evaluation of the renormalized quark mass, we investigate the validity of the diagonal and nondiagonal Goldberger-Treiman relations. The ratios $G_{\pi N\Delta}(q^2)/G_{\pi NN}(q^2)$ and $2C_5^A(q^2)/G_A(q^2)$ are constant as a function of the momentum transfer squared and show almost no dependence on the quark mass. We confirm equality of these two ratios consistent with the Goldberger-Treiman relations extracting a mean value of 1.61(2).

DOI: 10.1103/PhysRevD.76.094511 PACS numbers: 11.15.Ha, 12.38.Gc, 12.38.Aw, 12.38.−t

I. INTRODUCTION

Form factors measured in electromagnetic and weak processes are fundamental probes of hadron structure. Despite the long history of experimental [1] and theoretical studies [2] on nucleon electromagnetic form factors, new measurements of these quantities continue to reveal interesting features. The discrepancy between the ratio of the electric to magnetic nucleon form factors extracted via Rosenbluth separation and from recent polarization measurements is a well-known example. The transition form factors in $\gamma N \rightarrow \Delta$ have recently been measured [3,4] to high accuracy, paving the way for theoretical studies using chiral effective theories [5,6] and lattice QCD [7–9]. Compared to the electromagnetic form factors, the nucleon (N) and nucleon to Δ form factors connected to the axial-vector current are more difficult to measure and therefore less accurately known. An exception is the nucleon axial charge $g_A = G_A(0)$, which can be determined precisely from β-decay. Its q^2-dependence has been studied from neutrino scattering [10] or pion electroproduction [11,12]. On the other hand the nucleon induced pseudoscalar form factor, $G_p(q^2)$, is less well known. Muon capture and radiative muon capture are the main experimental sources of information [13]. Both $G_A(q^2)$ and $G_p(q^2)$ have been discussed within chiral effective theories [14,15]. The electroweak N to Δ transition form factors are even less studied. Using Adler's parametrization [16] the N to Δ matrix element of the axial-vector current can be written in terms of four form factors, two of which are suppressed [17]. The two dominant transition form factors, $C_5^A(q^2)$ and $C_6^A(q^2)$, are analogous to $G_A(q^2)$ and $G_p(q^2)$, respectively. Neutrino interactions in hydrogen and deuterium were studied [18] in an effort to extract information on these form factors. Experiments using electroproduction of the Δ resonance are under way [19] to measure the parity violating asymmetry in N to Δ, connected to leading order to the form factor $C_5^A(q^2)$. Theoretical input on these form factors is therefore very timely and important.

State-of-the-art lattice QCD calculations can yield model independent results on these axial form factors, thereby providing direct comparison with experiment. Lattice studies reflect the experimental situation regarding our knowledge of these form factors. There have been several recent studies on the electromagnetic nucleon [20–22] and N to Δ form factors [5–9]. There have also been several lattice evaluations of g_A [23–25], but only very recently lattice studies have began probing the q^2-dependence of the nucleon axial form factors [26,27] and the N to Δ transition form factors [28]. A notable exception is an early lattice study on the nucleon axial form factors carried out in the quenched approximation for rather heavy pion masses [29].

In this work we calculate the nucleon axial form factors using Wilson fermions in the quenched theory and with two degenerate flavors of Wilson fermions [30,31]. The lowest pion mass in the case of dynamical Wilson fermions that we use is about 380 MeV. We also evaluate the pion-nucleon (πNN) form factor $G_{\pi NN}(q^2)$. For the extraction of this form factor we need the renormalized quark mass, which we calculate via the axial Ward-Takahashi identity (AWI). In addition, we present results on the dominant axial N to Δ transition form factors $C_6^A(q^2)$ and $C_5^A(q^2)$. The pion-nucleon-Δ ($\pi N\Delta$) form factor, $G_{\pi N\Delta}(q^2)$, is also computed in an analogous way to the evaluation of $G_{\pi NN}(q^2)$. Like in the case of the nucleon axial form

factors, the starting point is an evaluation in the quenched theory using the standard Wilson action. A quenched calculation allows an efficient check of our lattice techniques by enabling a computation of the relevant quantities on a large lattice minimizing finite volume effects and obtaining accurate results at small momentum transfers reaching pion mass, m_π, down to about 410 MeV. In the case of the N to Δ transition, the light quark regime is studied in two ways: Besides using configurations with two degenerate flavors of dynamical Wilson fermions we use a hybrid combination of domain wall valence quarks, which have chiral symmetry on the lattice, and MILC configurations generated with three flavors of staggered sea quarks using the Asqtad improved action [32]. The effectiveness of this hybrid combination has recently been demonstrated in the successful precision calculation of the nucleon axial charge, g_A [23], as well as in our first evaluation of the N to Δ axial transition form factors [28,33]. Since Wilson fermions have discretization errors in the lattice spacing, a, of $\mathcal{O}(a)$ and break chiral symmetry whereas the hybrid action has discretization errors of $\mathcal{O}(a^2)$ and chirally symmetric valence fermions, agreement between calculations using these two lattice actions provides a nontrivial check of consistency of the lattice results. In this work we obtain results on the dominant axial N to Δ form factors C_5^A and C_6^A with improved statistics as compared to their evaluation in Refs [28,33].

The evaluation of the axial form factors as well as the πNN and $\pi N\Delta$ form factors allows us to check the Goldberger-Treiman relations. It is advantageous to calculate ratios of the nucleon elastic and transition form factors, since ratios have weak quark mass dependence and we expect them to be less sensitive to other lattice artifacts. In particular, it is useful to consider ratios for which the renormalized quark mass cancels since this eliminates one source of systematic error.

The paper is organized as follows: In Sec. II, we give the definition of the matrix elements that we consider in terms of the form factors on the hadronic level. In Sec. III, we give the lattice matrix elements on the quark level and in Sec. IV, we discuss how we extract the form factors from lattice measurements. In Sec. V, we present our results. Finally in Sec. VI, we summarize and conclude.

II. DEFINITION OF MATRIX ELEMENTS

To extract the form factors, we need to evaluate hadronic matrix elements of the form $\langle h'|\mathcal{O}_\mu|h\rangle$, where h and h' are the initial and final hadron states and $\mathcal{O}_\mu$ a current that couples to a quark. In all that follows, we assume isospin symmetry and take the mass of the u and d quarks to be equal. We consider nucleon-nucleon and nucleon-Δ matrix elements of the axial-vector and pseudoscalar currents defined by

$$A_\mu^a(x) = \bar{\psi}(x)\gamma_\mu\gamma_5\frac{\tau^a}{2}\psi(x), \quad P^a(x) = \bar{\psi}(x)\gamma_5\frac{\tau^a}{2}\psi(x), \quad (1)$$

where τ^a are the three Pauli matrices acting in flavor space and ψ the isospin doublet quark field.

A. Axial form factors

The matrix element of the weak axial-vector current between nucleon states can be written in the form

$$\langle N(p',s')|A_\mu^3|N(p,s)\rangle = i\left(\frac{m_N^2}{E_N(\mathbf{p}')E_N(\mathbf{p})}\right)^{1/2}\bar{u}(p',s') \times\left[G_A(q^2)\gamma_\mu\gamma_5 + \frac{q_\mu\gamma_5}{2m_N}G_p(q^2)\right]\frac{\tau^3}{2}u(p,s), \quad (2)$$

where we specifically consider the axial isovector current A_μ^3. The form factors depend only on the momentum transfer squared, $q^2 = (p'_\mu - p_\mu)(p'^\mu - p^\mu)$. As defined above, the form factors $G_A(q^2)$ and $G_p(q^2)$ are dimensionless. As already mentioned in the introduction, there exist several recent lattice studies on the nucleon axial charge g_A [23–25], whereas only very recently there are lattice studies to investigate the q^2 dependence of $G_A(q^2)$ or $G_p(q^2)$, apart from an early calculation in the quenched approximation [29].

The invariant proton to Δ^+ weak matrix element is expressed in terms of four transition form factors [16,34] as

$$\langle\Delta(p',s')|A_\mu^3|N(p,s)\rangle = i\sqrt{\frac{2}{3}}\left(\frac{m_\Delta m_N}{E_\Delta(\mathbf{p}')E_N(\mathbf{p})}\right)^{1/2}\bar{u}^\lambda_{\Delta^+}(p',s') \times\left[\left(\frac{C_3^A(q^2)}{m_N}\gamma^\nu + \frac{C_4^A(q^2)}{m_N^2}p'^\nu\right) \times(g_{\lambda\mu}g_{\rho\nu} - g_{\lambda\rho}g_{\mu\nu})q^\rho + C_5^A(q^2)g_{\lambda\mu} + \frac{C_6^A(q^2)}{m_N^2}q_\lambda q_\mu\right]u_P(p,s) \quad (3)$$

where, as in the nucleon case, we consider the physically relevant axial isovector current $A_\mu^3(x)$. By u_P and $u^\lambda_{\Delta^+}$ we denote proton and Δ^+ spinors.

B. Pseudoscalar matrix elements

Spontaneous symmetry breaking couples pions to the broken axial charges and currents. The relation

$$\langle 0|A_\mu^a(0)|\pi^b(p)\rangle = if_\pi p_\mu\delta^{ab} \quad (4)$$

can be used to extract the pion decay constant, f_π, on the lattice by evaluating two-point functions. With our conventions $f_\pi = 92$ MeV. Taking the divergence of the axial-vector current we obtain the operator relation

$$\partial^\mu A_\mu^a = f_\pi m_\pi^2\pi^a, \quad (5)$$

known as the partially conserved axial-vector current

(PCAC) hypothesis. On the QCD level we have the axial Ward-Takahashi identity

$$\partial^\mu A^a_\mu = 2m_q P^a, \tag{6}$$

where all quantities appearing in Eq. (6) are renormalized quantities with m_q being the renormalized quark mass. Comparing Eqs. (5) and (6) we can write the pion field π^a in terms of the pseudoscalar density as

$$\pi^a = \frac{2m_q P^a}{f_\pi m_\pi^2}. \tag{7}$$

The renormalized quark mass can be evaluated by taking the matrix element of Eq. (6) between a zero momentum pion state and the vacuum to obtain

$$m_q = \frac{m_\pi \langle 0|A^a_0|\pi^a(0)\rangle}{2\langle 0|P^a|\pi^a(0)\rangle}. \tag{8}$$

Taking the matrix element of the pseudoscalar density between nucleon states we can define the πNN form factor via

$$\begin{aligned} 2m_q\langle N(p',s')|P^3|N(p,s)\rangle = &\left(\frac{m_N^2}{E_N(\mathbf{p}')E_N(\mathbf{p})}\right)^{1/2} \\ &\times \frac{f_\pi m_\pi^2 G_{\pi NN}(q^2)}{m_\pi^2 - q^2} \\ &\times \bar{u}(p',s') i\gamma_5 \frac{\tau^3}{2} u(p,s). \end{aligned} \tag{9}$$

Similarly the proton-Δ^+ matrix element of the pseudoscalar density yields the $\pi N\Delta$ form factor:

$$\begin{aligned} 2m_q\langle \Delta(p',s')|P^3|N(p,s)\rangle = &\, i\sqrt{\frac{2}{3}}\left(\frac{m_\Delta m_N}{E_\Delta(\mathbf{p}')E_N(\mathbf{p})}\right)^{1/2} \\ &\times \frac{f_\pi m_\pi^2 G_{\pi N\Delta}(q^2)}{m_\pi^2 - q^2} \bar{u}^\nu_{\Delta^+}(p',s') \\ &\times \frac{q_\nu}{2m_N} u_P(p,s). \end{aligned} \tag{10}$$

Equations (9) and (10) define the form factors $G_{\pi NN}(q^2)$ and $G_{\pi N\Delta}(q^2)$ that we study in this work. The πNN and $\pi N\Delta$ strong coupling constants are then given by $g_{\pi NN} = G_{\pi NN}(0)$ and $g_{\pi N\Delta} = G_{\pi N\Delta}(0)$. PCAC relates the axial form factors $G_A(q^2)$ and $G_p(q^2)$ with $G_{\pi NN}(q^2)$ and equivalently $C_5^A(q^2)$ and $C_6^A(q^2)$ with $G_{\pi N\Delta}(q^2)$. Using the PCAC hypothesis together with Eq. (9) we obtain the diagonal Goldberger-Treiman relation (GTR)

$$G_A(q^2) + \frac{q^2}{4m_N^2} G_p(q^2) = \frac{1}{2m_N} \frac{2G_{\pi NN}(q^2) f_\pi m_\pi^2}{m_\pi^2 - q^2}. \tag{11}$$

Similarly using Eq. (10) we obtain the nondiagonal GTR

$$C_5^A(q^2) + \frac{q^2}{m_N^2} C_6^A(q^2) = \frac{1}{2m_N} \frac{G_{\pi N\Delta}(q^2) f_\pi m_\pi^2}{m_\pi^2 - q^2}. \tag{12}$$

Assuming pion pole dominance we can relate the form factors $G_p(q^2)$ to $G_{\pi NN}(q^2)$ and $C_6^A(q^2)$ to $G_{\pi N\Delta}(q^2)$ via

$$\begin{aligned} \frac{1}{2m_N} G_p(q^2) &\sim \frac{2G_{\pi NN}(q^2) f_\pi}{m_\pi^2 - q^2}, \\ \frac{1}{m_N} C_6^A(q^2) &\sim \frac{1}{2} \frac{G_{\pi N\Delta}(q^2) f_\pi}{m_\pi^2 - q^2}. \end{aligned} \tag{13}$$

Substituting in Eqs. (11) and (12) we obtain the simplified Goldberger-Treiman relations

$$\begin{aligned} f_\pi G_{\pi NN}(q^2) &= m_N G_A(q^2), \\ f_\pi G_{\pi N\Delta}(q^2) &= 2m_N C_5^A(q^2). \end{aligned} \tag{14}$$

III. LATTICE EVALUATION OF CORRELATION FUNCTIONS

To evaluate the axial nucleon form factors $G_A(q^2)$ and $G_p(q^2)$, we use the techniques developed in our study of the nucleon isovector electromagnetic form factors [22]. Since only the axial isovector is of relevance here, only the connected diagram shown in Fig. 1 is needed. To extract the matrix element of the axial isovector current between nucleon states defined in Eq. (2) we need to calculate the three-point function

$$\begin{aligned} &\langle G^{NA^3_\mu N}(t_2,t_1;\mathbf{p}',\mathbf{p};\Gamma)\rangle \\ &\quad = \sum_{\mathbf{x}_2,\mathbf{x}_1} \exp(-i\mathbf{p}'\cdot\mathbf{x}_2)\exp(+i(\mathbf{p}'-\mathbf{p})\cdot\mathbf{x}_1) \\ &\qquad \times \Gamma^{\beta\alpha}\langle\Omega|T[\chi^\alpha(\mathbf{x}_2,t_2)A^3_\mu(\mathbf{x}_1,t_1)\bar{\chi}^\beta(\mathbf{0},0)]|\Omega\rangle, \end{aligned} \tag{15}$$

using the local quark bilinear axial current $A^3_\mu(x)$ of Eq. (1). The projection matrices for the Dirac indices are given by

$$\Gamma_i = \frac{1}{2}\begin{pmatrix} \sigma_i & 0 \\ 0 & 0 \end{pmatrix}, \qquad \Gamma_4 = \frac{1}{2}\begin{pmatrix} I & 0 \\ 0 & 0 \end{pmatrix}. \tag{16}$$

An interpolating field with the quantum numbers of the nucleon routinely used in lattice studies is

$$\chi(x) = \epsilon^{abc}[u^{Ta}(x)C\gamma_5 d^b(x)]u^c(x). \tag{17}$$

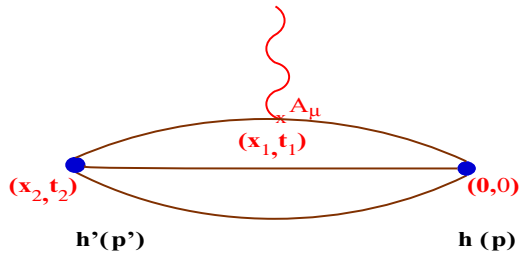

FIG. 1 (color online). Connected three-point function between final and initial hadron states $h'(\mathbf{p}')$ and $h(\mathbf{p})$.

We create an initial state (source) by acting with $\bar{\chi}(0)$ on the vacuum. Evolution in Euclidean time with the QCD Hamiltonian produces, in the large time limit, the nucleon state. We take t_1, the time from the source at which the axial-vector current couples to a quark, to be large enough so that the nucleon is the dominant state. We then take the overlap with a nucleon state that is annihilated at a later time $t_2 - t_1$ by the same interpolating field $\chi(x_2)$ (sink). Again $t_2 - t_1$ is large enough so that the nucleon is the dominant state. This process is schematically shown in Fig. 1. In addition, we calculate the nucleon two-point function,

$$\langle G^{NN}(t, \mathbf{p}; \Gamma)\rangle = \sum_{\mathbf{x}} e^{-i\mathbf{p}\cdot\mathbf{x}} \Gamma^{\beta\alpha} \langle \Omega | T \chi^{\alpha}(\mathbf{x}, t) \bar{\chi}^{\beta}(\mathbf{0}, 0) | \Omega \rangle. \tag{18}$$

We then construct a ratio such that, in the large Euclidean time limit, all exponential dependences on times and unknown initial state-nucleon overlap constants $\langle N|\bar{\chi}|0\rangle$ cancel. One can construct more than one ratio that accomplishes this. We require, in addition, that we use two-point functions that involve the shortest time evolution. Such a ratio is given by

$$R^A(t_2, t_1; \mathbf{p}', \mathbf{p}; \Gamma; \mu) = \frac{\langle G^{NA^3_\mu N}(t_2, t_1; \mathbf{p}', \mathbf{p}; \Gamma)\rangle}{\langle G^{NN}(t_2, \mathbf{p}'; \Gamma_4)\rangle} \left[\frac{\langle G^{NN}(t_2 - t_1, \mathbf{p}; \Gamma_4)\rangle \langle G^{NN}(t_1, \mathbf{p}'; \Gamma_4)\rangle \langle G^{NN}(t_2, \mathbf{p}'; \Gamma_4)\rangle}{\langle G^{NN}(t_2 - t_1, \mathbf{p}'; \Gamma_4)\rangle \langle G^{NN}(t_1, \mathbf{p}; \Gamma_4)\rangle \langle G^{NN}(t_2, \mathbf{p}; \Gamma_4)\rangle} \right]^{1/2} \overset{t_2 - t_1 \gg 1, t_1 \gg 1}{\Rightarrow} \Pi^A(\mathbf{p}', \mathbf{p}; \Gamma; \mu), \tag{19}$$

which, in the large Euclidean time when the nucleon is the dominant state, produces a constant plateau region in t_1. Throughout this work we use kinematics where the final hadron state is produced at rest and therefore the momentum transfer $\mathbf{q} = \mathbf{p}' - \mathbf{p} = -\mathbf{p}$. We take $-q^2 = Q^2 > 0$ with Q^2 being the Euclidean momentum transfer squared. The value of $R^A(t_2, t_1; \mathbf{p}', \mathbf{p}; \Gamma; \mu)$ in the plateau region, $\Pi^A(\mathbf{p}', \mathbf{p}; \Gamma; \mu)$, is directly connected to the nucleon form factors through the relation

$$\Pi^A(\mathbf{0}, -\mathbf{q}; \Gamma_k; \mu) = i \frac{C}{4m_N} \Big[((E_N + m_N)\delta_{k,\mu} + q_k \delta_{\mu,4}) G_A(Q^2) - \frac{q_\mu q_k}{2m_N} G_p(Q^2) \Big] \tag{20}$$

for $k = 1, 2, 3$, while $\Pi^A(\mathbf{0}, -\mathbf{q}; \Gamma_4; \mu) = 0$. The nucleon energy $E_N = \sqrt{m_N^2 + \mathbf{q}^2}$ and $C = \sqrt{\frac{2m_N^2}{E_N(E_N + m_N)}}$, a factor related to the normalization of the lattice states. Since our goal is to evaluate the form factors as a function of Q^2, we calculate the three-point functions with sequential inversions through the sink. This requires fixing the source-sink time separation t_2 as well as the initial and final hadron states but allows the insertion of any operator with arbitrary momentum at any time slice t_1. In fact, the usefulness of this technique is evident in this work: Since the same matrix elements were calculated for the electromagnetic current [8,9,22] *no new sequential inversions* are required for the axial current or pseudoscalar density operators.

As in the electromagnetic case, it is advantageous to use a linear combination of nucleon interpolating fields to construct optimal sources and sinks. Since for axial operators a nonzero contribution can be obtained only if $\Gamma \neq \Gamma_4$ in the three-point function, the most symmetric linear combination of matrix elements that can be considered is

$$S^A(\mathbf{q}; j) = \sum_{k=1}^{3} \Pi^A(\mathbf{0}, -\mathbf{q}; \Gamma_k; \mu = j) = i \frac{C}{4m_N} \Big[(E_N + m_N)(\delta_{1,j} + \delta_{2,j} + \delta_{3,j}) G_A(Q^2) - (q_1 + q_2 + q_3) \frac{q_j}{2m_N} G_p(Q^2) \Big], \tag{21}$$

where $j = 1, 2, 3$ labels the spatial current direction. In order to obtain the three matrix elements corresponding to three choices of Γ_k in the above sum one would require three sequential inversions. However, choosing an appropriate linear combination of nucleon interpolating fields, this sum is automatically built in and with one sequential inversion we can obtain $S^A(\mathbf{q}; j)$ for all current directions j. We call such a linear combination optimal sink because it allows us to take into account in our determination of the form factors the largest set of momentum vectors contributing to the same Q^2 value. Since the sequential propagators corresponding to this sink have been computed for the isovector electromagnetic form factors [22] they can be used directly here. Therefore, the computational cost for the evaluation of the three-point function for all intermediate times t_1, current indices μ, and a large set of lattice momenta vectors $\mathbf{q}$ is very small.

Similarly, to evaluate the πNN form factor $G_{\pi NN}$ we construct the ratio R^P, which is the same as the ratio R^A given in Eq. (19) but instead of the three-point function $\langle G^{NA^3_\mu N}(t_2, t_1; \mathbf{p}', \mathbf{p}; \Gamma)\rangle$ defined in Eq. (15) with the axial current A^3_μ, we use the three-point function $\langle G^{NP^3N}(t_2, t_1; \mathbf{p}', \mathbf{p}; \Gamma)\rangle$, obtained by replacing A^3_μ in Eq. (15) by the pseudoscalar density P^3. The large Euclidean time behavior of R^P is independent of t_1 leading to the plateau value denoted by $\Pi^P(\mathbf{0}, -\mathbf{q}; \Gamma; \gamma_5)$. The value of R^P in the plateau region, Π^P, is related to the πNN form factor via

$$\Pi^P(\mathbf{0}, -\mathbf{q}; \Gamma_k; \gamma_5) = C\frac{q_k}{2m_N}\frac{f_\pi m_\pi^2}{2m_q(m_\pi^2 + Q^2)}G_{\pi NN}(Q^2) \tag{22}$$

for $k = 1, 2, 3$ while $\Pi^P(\mathbf{0}, -\mathbf{q}; \Gamma_4; \gamma_5) = 0$. Summation over the polarized matrix elements now leads to

$$\begin{aligned} S^P(\mathbf{q}; \gamma_5) &= \sum_{k=1}^{3} \Pi^P(\mathbf{0}, -\mathbf{q}; \Gamma_k; \gamma_5) \\ &= C\frac{q_1 + q_2 + q_3}{2m_N}\frac{f_\pi m_\pi^2}{2m_q(m_\pi^2 + Q^2)}G_{\pi NN}(Q^2), \end{aligned} \tag{23}$$

from which $G_{\pi NN}$ can be extracted if we know f_π and m_q.

The determination of the N to Δ axial transition form factors requires the evaluation of the three-point function

$$\begin{aligned} &\langle G_\sigma^{\Delta A_\mu^3 N}(t_2, t_1; \mathbf{p}', \mathbf{p}; \Gamma)\rangle \\ &\quad = \sum_{\mathbf{x}_2, \mathbf{x}_1} \exp(-i\mathbf{p}' \cdot \mathbf{x}_2)\exp(+i(\mathbf{p}' - \mathbf{p}) \cdot \mathbf{x}_1) \\ &\qquad \times \Gamma^{\beta\alpha}\langle\Omega|T[\chi_\sigma^\alpha(\mathbf{x}_2, t_2)A_\mu^3(\mathbf{x}_1, t_1)\bar{\chi}^\beta(\mathbf{0}, 0)]|\Omega\rangle, \end{aligned} \tag{24}$$

where to create an initial state with the Δ^+ quantum numbers we use the standard Rarita-Schwinger interpolating field

$$\begin{aligned} \chi_\sigma^{\Delta^+}(x) = \frac{1}{\sqrt{3}}\epsilon^{abc}\{&2[u^{Ta}(x)C\gamma_\sigma d^b(x)]u^c(x) \\ &+ [u^{Ta}(x)C\gamma_\sigma u^b(x)]d^c(x)\}. \end{aligned} \tag{25}$$

Besides the nucleon two-point function we also need the Δ two-point function given by

$$\langle G_{\sigma\tau}^{\Delta\Delta}(t, \mathbf{p}'; \Gamma)\rangle = \sum_{\mathbf{x}} e^{-i\mathbf{p}'\cdot\mathbf{x}}\Gamma^{\beta\alpha}\langle\Omega|T\chi_\sigma^\alpha(\mathbf{x}, t)\bar{\chi}_\tau^\beta(\mathbf{0}, 0)|\Omega\rangle. \tag{26}$$

The corresponding ratio which, in the large Euclidean time limit, becomes t_1-independent, is given by

$$\begin{aligned} &R_\sigma^A(t_2, t_1; \mathbf{p}', \mathbf{p}; \Gamma; \mu) \\ &\quad = \frac{\langle G_\sigma^{\Delta A_\mu^3 N}(t_2, t_1; \mathbf{p}', \mathbf{p}; \Gamma)\rangle}{\langle G_{ii}^{\Delta\Delta}(t_2, \mathbf{p}'; \Gamma_4)\rangle}\left[\frac{\langle G_{ii}^{\Delta\Delta}(t_2, \mathbf{p}'; \Gamma_4)\rangle}{\langle G^{NN}(t_2, \mathbf{p}; \Gamma_4)\rangle}\right. \\ &\qquad \left.\times \frac{\langle G^{NN}(t_2 - t_1, \mathbf{p}; \Gamma_4)\rangle\langle G_{ii}^{\Delta\Delta}(t_1, \mathbf{p}'; \Gamma_4)\rangle}{\langle G_{ii}^{\Delta\Delta}(t_2 - t_1, \mathbf{p}'; \Gamma_4)\rangle\langle G^{NN}(t_1, \mathbf{p}; \Gamma_4)\rangle}\right]^{1/2} \\ &\quad \overset{t_2 - t_1 \gg 1, t_1 \gg 1}{\Rightarrow} \Pi_\sigma^A(\mathbf{p}', \mathbf{p}; \Gamma; \mu). \end{aligned} \tag{27}$$

As in the nucleon case, we take the final Δ state to be produced at rest and therefore $\mathbf{q} = \mathbf{p}' - \mathbf{p} = -\mathbf{p}$. The value of R_σ^A in the plateau region, Π_σ^A, for the case $\Gamma = \Gamma_4$, which is the relevant one for this work, is related to the form factors via

$$\begin{aligned} \Pi_k^A(\mathbf{0}, -\mathbf{q}; \Gamma_4; j) = iB\Bigg[&-\left\{\frac{(E_N - 2m_\Delta + m_N)}{2}\delta_{k,j}\right. \\ &\left.+ \frac{p^k p^j}{2(E_N + m_N)}\right\}C_3^A \\ &- \left\{(E_N - m_\Delta)\frac{m_\Delta}{m_N}\delta_{k,j}\right\}C_4^A \\ &+ m_N\delta_{k,j}C_5^A - \frac{p^k p^j}{m_N}C_6^A\Bigg] \end{aligned} \tag{28}$$

for the spatial components of the current, $\mu = j$, whereas for the temporal current component, $\mu = 4$, we have

$$\Pi_k^A(\mathbf{0}, -\mathbf{q}; \Gamma_4; 4) = Bp^k\left[C_3^A + \frac{m_\Delta}{m_N}C_4^A + \frac{E_N - m_\Delta}{m_N}C_6^A\right], \tag{29}$$

for $k = 1, 2, 3$, while $\Pi_4(0, -\mathbf{q}; \Gamma; \mu) = 0$. In this case we have a larger freedom in choosing appropriate linear combinations for the optimal sink due to the additional vector index of the Δ. Using this freedom we construct Δ sinks so that the maximum allowed number of lattice vectors contribute in the evaluation of the form factors at a given value of Q^2. These turn out to be the same as the ones used in our study of the N to Δ electromagnetic transition form factors [8]. Therefore the sequential inversions already performed for the evaluation of the N to Δ electromagnetic transition form factors [8,9] can be used for the computation of the axial transition form factors. We give below the expressions that we obtain in the large Euclidean time limit, using the optimal linear combinations of Δ interpolating fields:

$$\begin{aligned} S_1^A(\mathbf{q}; j) &= \sum_{\sigma=1}^{3}\Pi_\sigma^A(\mathbf{0}, -\mathbf{q}; \Gamma_4; j) \\ &= iB\Bigg[-\frac{C_3^A}{2}\Bigg\{(E_N - 2m_\Delta + m_N) \\ &\quad + \left(\sum_{k=1}^{3}p^k\right)\frac{p^j}{E_N + m_N}\Bigg\} - \frac{m_\Delta}{m_N}(E_N - m_\Delta)C_4^A \\ &\quad + m_N C_5^A - \frac{C_6^A}{m_N}p^j\left(\sum_{k=1}^{3}p^k\right)\Bigg], \end{aligned} \tag{30}$$

$$\begin{aligned} S_1^A(\mathbf{q}; 4) &= \sum_{\sigma=1}^{3}\Pi_\sigma^A(\mathbf{0}, -\mathbf{q}; \Gamma_4; 4) \\ &= B\sum_{k=1}^{3}p^k\left[C_3^A + \frac{m_\Delta}{m_N}C_4^A + \frac{E_N - m_\Delta}{m_N}C_6^A\right], \end{aligned} \tag{31}$$

$$S_2^A(\mathbf{q};j) = \sum_{\sigma\neq k=1}^{3} \Pi_\sigma^A(\mathbf{0},-\mathbf{q};\Gamma_k;j)$$
$$= i\frac{3A}{2}\Big[\Big(\sum_{k=1}^{3} p^k\Big)(\delta_{j,1}(p^2-p^3) + \delta_{j,2}(p^3-p^1) + \delta_{j,3}(p^1-p^2))C_3^A\Big], \quad (32)$$

$$S_3^A(\mathbf{q};j) = \Pi_3^A(\mathbf{0},-\mathbf{q};\Gamma_3;\mu) - \frac{1}{2}[\Pi_1^A(\mathbf{0},-\mathbf{q};\Gamma_1;\mu).. + \Pi_2^A(\mathbf{0},-\mathbf{q};\Gamma_2;\mu)]$$
$$= iA\Big[\frac{9}{4}(\delta_{j,1}p^2p^3 - \delta_{j,2}p^1p^3)C_3^A\Big], \quad (33)$$

where $j = 1, 2, 3$ and

$$A = \frac{B}{(E_N+m_N)}, \qquad B = \sqrt{\frac{2}{3}}\frac{\sqrt{(E_N+m_N)/E_N}}{3m_N}. \quad (34)$$

As can be seen, $S_2^A(\mathbf{q};j)$ and $S_3^A(\mathbf{q};j)$ isolate the suppressed form factor C_3^A for different combinations of lattice momentum vectors as compared to S_1^A that also involves C_3^A. Since here we are only interested in the dominant form factors C_5^A and C_6^A, we use only $S_1^A(\mathbf{q};\mu)$. By $R_{N\Delta}^A$, we denote the ratio constructed analogously to R_σ^A, but with the optimal sink. The linear combination $S_1^A(\mathbf{q};\mu)$ turns out to be the suitable one also for the calculation of the form factor $G_{\pi N\Delta}$, defined in Eq. (10). Again replacing the three-point function $\langle G_\sigma^{\Delta A_\mu^3 N}(t_2,t_1;\mathbf{p}',\mathbf{p};\Gamma)\rangle$ with the corresponding pseudoscalar three-point function $\langle G_\sigma^{\Delta P^3 N}(t_2,t_1;\mathbf{p}',\mathbf{p};\Gamma)\rangle$ in Eq. (27), we obtain the ratio R_σ^P, which at large Euclidean times becomes time-independent. Fitting in the plateau region yields $\Pi_\sigma^P(\mathbf{0},-\mathbf{q};\Gamma;\gamma_5)$, related to the $\pi N\Delta$ form factor via the relation

$$\Pi_\sigma^P(\mathbf{0},-\mathbf{q};\Gamma_4;\gamma_5) = \sqrt{\frac{2}{3}}\sqrt{\frac{E_N+m_N}{E_N}}\frac{q_\sigma}{6m_N} \times \frac{f_\pi m_\pi^2}{2m_q(m_\pi^2+Q^2)}G_{\pi N\Delta}(Q^2). \quad (35)$$

The optimal combination gives

$$S_{N\Delta}^P(\mathbf{q};\gamma_5) = \sum_{\sigma=1}^{3}\Pi_\sigma^P(\mathbf{0},-\mathbf{q};\Gamma_4;\gamma_5)$$
$$= \sqrt{\frac{2}{3}}\sqrt{\frac{E_N+m_N}{E_N}}\Big[\frac{q_1+q_2+q_3}{6m_N} \times \frac{f_\pi m_\pi^2}{2m_q(m_\pi^2+Q^2)}\Big]G_{\pi N\Delta}(Q^2), \quad (36)$$

from which $G_{\pi N\Delta}$ can be determined.

In order to evaluate $G_{\pi NN}$ and $G_{\pi N\Delta}$, we need to know m_q. The renormalized quark mass can be defined via the AWI given in Eq. (8). On the lattice the AWI has corrections, which in the case of Wilson fermions are of order a. For domain wall fermions (DWF), the divergence of the four-dimensional vector axial current has an additional term that goes to zero as the fifth dimension goes to infinity [35]. For nonsinglet matrix elements at low energies, this additional term shifts the quark mass by an additive constant known as the residual quark mass [36]. Such a simple shift is valid up to order a^2. Provided that the fifth dimension is large enough, the residual mass maybe considered a small correction. The size of the fifth dimension was adjusted by requiring the residual mass to be small compared to the pion mass. The criterion used to fix the fifth dimension to 16 is that the residual mass is smaller than 10% of the quark mass [37]. We adopt the same criterion in this work and take the fifth dimension to be 16. Therefore we assume that corrections due to the residual mass are small and we calculate the renormalized quark mass using the AWI taking matrix elements between a pion zero momentum state and the vacuum. The initial state with the pion quantum numbers is created using the axial-vector current $\tilde{A}_4^3$ as an interpolating field. Quantities with tildes denote operators that are built from smeared quark fields obtained from point quark fields $\psi(x)$ as described in the next subsection. The pion-vacuum matrix element of the axial-vector current is given by the two-point function

$$C_{\mathrm{LS}}^A(t) = \sum_{\mathbf{x}}\langle\Omega|T(A_4^3(\mathbf{x},t)\tilde{A}_4^3(\mathbf{0},0))|\Omega\rangle \quad (37)$$

and the pion-vacuum matrix element of the pseudoscalar density is given by

$$C_{\mathrm{LS}}^P(t) = \sum_{\mathbf{x}}\langle\Omega|T(P^3(\mathbf{x},t)\tilde{P}^3(\mathbf{0},0))|\Omega\rangle. \quad (38)$$

The subscripts L and S denote that the axial-vector current and pseudoscalar density are constructed using local quark fields unlike the interpolating fields $\tilde{A}_4^3$ and $\tilde{P}^3$ that use smeared quark fields. To cancel the overlaps of our initial pion state with the vacuum we form the ratio

$$m_{\mathrm{eff}}^{\mathrm{AWI}}(t) = \frac{m_\pi}{2}\frac{Z_A}{Z_P}\frac{C_{\mathrm{LS}}^A(t)}{C_{\mathrm{LS}}^P(t)}\sqrt{\frac{C_{\mathrm{SS}}^P(t)}{C_{\mathrm{SS}}^A(t)}} \quad (39)$$

using, in addition to local-smeared (LS) two-point functions, the smeared-smeared two-point functions C_{SS}^A and C_{SS}^P. We look for a plateau in the large Euclidean time behavior of the effective mass $m_{\mathrm{eff}}(t)$, which determines m_q. The factors Z_A and Z_P are the renormalization constants for the local axial-vector and pseudoscalar currents, respectively. We note that Z_P is only needed for the determination of the renormalized quark mass. This dependence cancels in all physical quantities presented in this work, which are therefore independent of the value we use for Z_P. The evaluation of m_q together with the determination of f_π

TABLE I. Parameters for the calculations using Wilson fermions.

Wilson fermions Number of confs	κ	m_π (GeV)	m_N (GeV)	m_Δ (GeV)
Quenched $32^3 \times 64$, $\beta = 6.0$, $a^{-1} = 2.14(6)$ GeV				
200	0.1554	0.563(4)	1.267(11)	1.470(15)
200	0.1558	0.490(4)	1.190(13)	1.425(16)
200	0.1562	0.411(4)	1.109(13)	1.382(19)
	$\kappa_c = 0.1571$	0	0.938(9)	
Unquenched [30] $24^3 \times 40$, $\beta = 5.6$, $a^{-1} = 2.56(10)$ GeV				
185	0.1575	0.691(8)	1.485(18)	1.687(15)
157	0.1580	0.509(8)	1.280(26)	1.559(19)
Unquenched [31] $24^3 \times 32$, $\beta = 5.6$, $a^{-1} = 2.56(10)$ GeV				
200	0.15825	0.384(8)	1.083(18)	1.395(18)
	$\kappa_c = 0.1585$	0	0.938(33)	

allows us to evaluate $G_{\pi NN}$ and $G_{\pi N\Delta}$. The pion decay constant f_π is determined from the large Euclidean time behavior of the ratio

$$f_\pi^{\text{eff}}(t) = Z_A \sqrt{\frac{2}{m_\pi}} \frac{C^A_{\text{LS}}(t)}{\sqrt{C^A_{\text{SS}}(t)}} e^{m_\pi t/2}. \tag{40}$$

For large t, the above quantity becomes t independent and the plateau value gives f_π.

In the case of Wilson fermions the evaluation of N to Δ matrix elements is done using the sequential propagators already computed in our study of the electromagnetic transition form factors [8,9]. On the other hand, in the hybrid scheme, additional propagators are calculated to improve the statistical errors beyond those of our previous work [9,28] and to check for finite volume effects. We summarize in Tables I and II the details of the calculation. All the hadron masses given in Table II are computed using domain wall valence quarks and MILC configurations for the sea quarks. The value of the valence domain wall quark mass, m_q^{DW}, was determined by tuning the pion mass calculated with domain wall fermions to be the same as the lowest mass pion in the staggered formulation [37].

For Wilson fermions, we convert dimensionless lattice quantities to physical units by setting the lattice spacing using the nucleon mass at the chiral limit. The value of a extracted from the nucleon mass is given in Table I and it is consistent with the value extracted using the Sommer scale r_0. The dynamical Wilson configurations at $\kappa = 0.1575$ and 0.1580 were generated by the $T\chi L$ collaboration [30] and at $\kappa = 0.158\,25$ by the DESY-Zeuthen group [31]. For the hybrid calculation we use the scale extracted from heavy meson spectroscopy as determined by the MILC collaboration [38]. As can be seen in Table II in the hybrid approach we consider lattices with temporal extent 32 and 64. Temporal extent 32 is obtained by using Dirichlet boundary conditions (b.c.) in the temporal direction to cut into half the original MILC lattices when we calculate the domain wall quark propagator. This was the procedure adopted in our previous evaluation of N to Δ axial form factors [9] due to the limited computer resources. In this work we present, in addition, results using the full temporal extent of the MILC lattices with antiperiodic b.c. in the temporal direction consistent with what is used in the simulation of the configurations. Antiperiodic b.c. in the temporal direction are also used in the case of Wilson fermions.

IV. EXTRACTION OF OBSERVABLES

A. Ground state dominance and noise reduction

As we already pointed out, in order to extract physical matrix elements, we must first evolve in Euclidean time to create the hadronic state of interest. In this work, the

TABLE II. Parameters for the calculations using the hybrid action.

Hybrid action $a^{-1} = 1.58$ GeV [38] Number of confs	Volume	$(am_{u,d})^{\text{sea}}$	$(am_s)^{\text{sea}}$	$(am_q)^{\text{DW}}$	m_π (GeV)	m_N (GeV)	m_Δ (GeV)
150	$20^3 \times 32$	0.03	0.05	0.0478	0.606(2)	1.392(9)	1.670(22)
150	$20^3 \times 32$	0.02	0.05	0.0313	0.502(4)	1.255(19)	1.567(25)
118	$28^3 \times 32$	0.01	0.05	0.0138	0.364(1)	1.196(25)	1.561(41)
200	$20^3 \times 64$	0.03	0.05	0.0478	0.594(1)	1.416(20)	1.683(22)
198	$20^3 \times 64$	0.02	0.05	0.0313	0.498(3)	1.261(17)	1.589(35)
100	$20^3 \times 64$	0.01	0.05	0.0138	0.362(5)	1.139(25)	1.488(71)
300	$28^3 \times 64$	0.01	0.05	0.0138	0.353(2)	1.191(19)	1.533(27)

hadronic states of interest are the pion, the nucleon, and the Δ states. To create the initial states with the pion quantum numbers, we use the temporal component of the axial-vector current, and for the nucleon and Δ, the interpolating fields given in Eqs. (17) and (25) respectively. The length of the time evolution required to obtain the true pion, nucleon, and Δ eigenstates depends on our choice of the initial state. It is well known that if one constructs a hadron initial state using smeared quark fields instead of localized ones, the convergence to the hadron eigenstate is very much improved. Therefore, in this work, we always smear the quark fields in a gauge invariant way using the so-called Wuppertal or Gaussian smearing [39]. In this scheme the smeared quark field, $\tilde{\psi}(\mathbf{x}, t)$, is obtained from the localized field, $\psi(\mathbf{y}, t)$, via

$$\tilde{\psi}(\mathbf{x}, t) = \sum_{\mathbf{y}} F(\mathbf{x}, \mathbf{y}; U(t))\psi(\mathbf{y}, t). \tag{41}$$

The gauge invariant smearing function is constructed from the hopping matrix H:

$$F(\mathbf{x}, \mathbf{y}; U(t)) = (1 + \alpha H)^n(\mathbf{x}, \mathbf{y}; U(t)), \tag{42}$$

where

$$H(\mathbf{x}, \mathbf{y}; U(t)) = \sum_{i=1}^{3} (U_i(\mathbf{x}, t)\delta_{\mathbf{x},\mathbf{y}-i} + U_i^\dagger(\mathbf{x} - i, t)\delta_{\mathbf{x},\mathbf{y}+i}). \tag{43}$$

The parameters for the Wuppertal smearing are determined by requiring that the nucleon state dominates the two-point correlator for the shortest time evolution. We find that $\alpha = 4$ and $n = 50$ are optimal parameters. Although smearing improves ground state dominance, it introduces gauge noise increasing the errors on the extracted effective masses, in particular, when applied both to the source and to the sink. An efficient way to reduce the ultraviolet fluctuations is to smooth the gauge fields that enter the hopping matrix $H(\mathbf{x}, \mathbf{y}; U(t))$. It was shown in Ref. [22] that hypercubic (HYP) smearing [40] on these gauge links reduces gauge noise and tends to also improve ground state dominance. In the case of domain wall fermions, HYP smearing is in fact applied to all the gauge links so as to accelerate the convergence of the bi-conjugate gradient method used to evaluate the inverse of the fermionic matrix. In the quenched case, HYP smearing is not used because self-averaging is more effective on larger lattices. In the case of dynamical Wilson fermions, the simulations are done on smaller lattices causing gauge noise, and HYP smearing needs to be applied to the gauge fields that enter the hopping matrix $H(\mathbf{x}, \mathbf{y}; U(t))$.

B. Plateaus and overconstrained analysis

In this subsection we describe the analysis of the lattice measurements that lead to the extraction of physical quantities.

The mass of the lowest hadron state for a given set of quantum numbers is the simplest quantity to calculate on the lattice, since it requires only the computation of two-point functions. In this work, besides the pion, the nucleon, and the Δ mass, which are straightforward to determine, we need the renormalized quark mass. This is evaluated by taking matrix elements of the AWI as discussed in Sec. III. The effective mass $m_{\rm eff}^{\rm AWI}(t)$ defined in Eq. (39) becomes time-independent if t is large enough so that the pion ground state dominates (plateau region). We show in Fig. 2 $m_{\rm eff}^{\rm AWI}(t)$ as a function of time, both in lattice units. We consider all three values of the bare quark mass for each of the three types of simulations that we use in this work, namely, the quenched approximation, two dynamical Wilson fermions, and the hybrid scheme. As can be seen, in all cases, allowing for an initial time evolution, the effective mass becomes time-independent, yielding in the plateau region m_q. In the case of DWF, the extracted value is expected to be the same as $m_q^{\rm DW}$ used in the domain wall Dirac matrix and given in Table II. Any differences are attributed to an additive residual mass that provides a

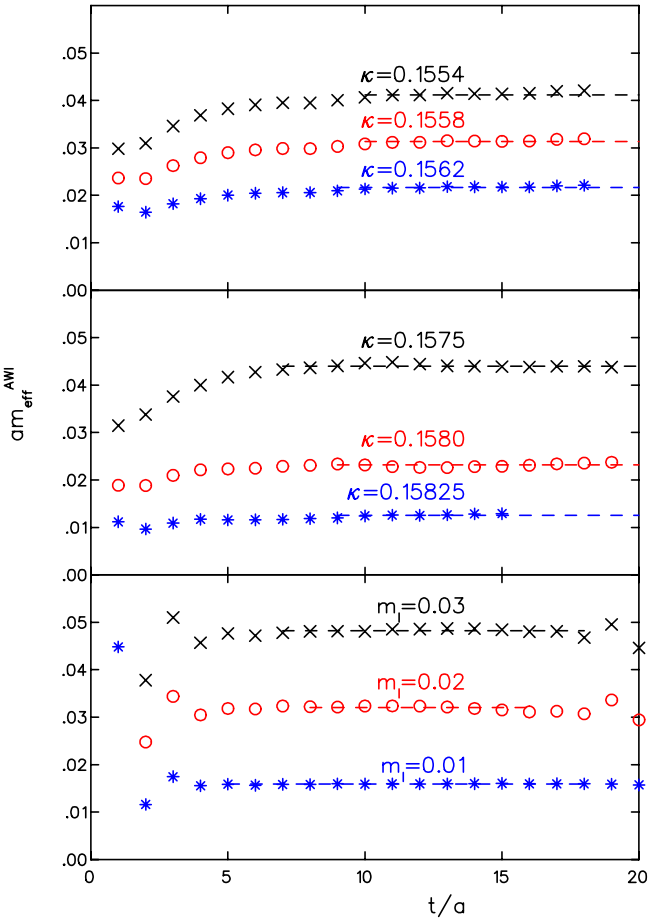

FIG. 2 (color online). The effective quark mass $m_{\rm eff}^{\rm AWI}(t)$ defined in Eq. (39) as a function of time, both in lattice units. The upper graph is for the quenched case, the middle graph for dynamical Wilson fermions, and the lower graph for the hybrid scheme. The dashed lines span the range of fitted points and show the extracted value of m_q in lattice units.

measure of the chiral symmetry breaking due to the finite extent of the fifth dimension. In the case of Wilson fermions it is known that the AWI has corrections of $\mathcal{O}(a)$. The value of m_q therefore carries systematic errors, which can be large as we approach the chiral limit, since corrections that appear in the right hand side of Eq. (6) will dominate as the first term decreases. The results on m_q will be discussed in the next section.

For the evaluation of form factors we look for time independence of the ratios R^A, R^P, $R^A_{N\Delta}$, and $R^P_{N\Delta}$ constructed from three-point functions and appropriate combinations of two-point functions. We start with the ratio $R^P \overset{t_1\gg 1, t_2-t_1\gg 1}{\longrightarrow} S^P$ from which the πNN form factor is determined. We show in Fig. 3 typical examples of the ratio R^P divided by $C(q_1+q_2+q_3)/2m_N$ and averaged over all momentum directions that lead to the same Q^2 value. A similar averaging is also done in our overconstrained analysis described below. The ratio is shown as a function of t_1 in physical units for the four lowest Q^2-values both in the quenched theory at the intermediate quark mass and for dynamical Wilson fermions at the heaviest quark mass. When the time separation from the source and sink is large enough so that the nucleon state dominates, this averaged ratio is indeed time-independent and the quantity plotted in Fig. 3 corresponds to $f_\pi m_\pi^2 G_{\pi NN}/[2m_q(Q^2+m_\pi^2)Z_P]$. Note that, since to obtain the renormalized mass we divide by Z_P, the Z_P factors cancel and therefore we do not need to know Z_P. As already pointed out, this is true for all physical quantities that we calculate in this work. The dashed lines show both the range used for the fit and the value of the plateau. In Fig. 4 we show the corresponding average of the ratio $R^P_{N\Delta}$ that, in the large time limit, leads to $S^P_{N\Delta}$ defined in Eq. (36) and to the determination of the $\pi N\Delta$ form factor. Here we show results for pions of mass of about 500 MeV (intermediate value) in each of the three types of simulations considered in this work. As can be seen the quality of the plateaus in all cases is good enough to allow us to fit to a

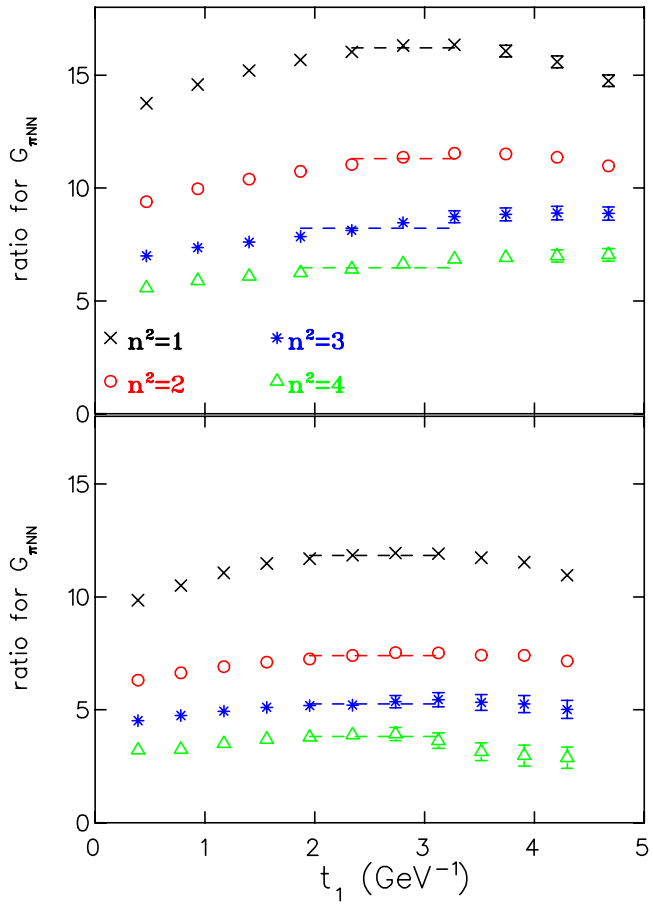

FIG. 3 (color online). The ratio R^P used to extract $G_{\pi NN}$ for the four lowest values of Q^2. The upper graph is for the quenched theory at $\kappa = 0.1558$ ($m_\pi = 0.49$ GeV) and the lower graph for dynamical Wilson fermions at $\kappa = 0.1575$ ($m_\pi = 0.69$ GeV). The dashed lines are fits to the plateaus and span the range of fitted points.

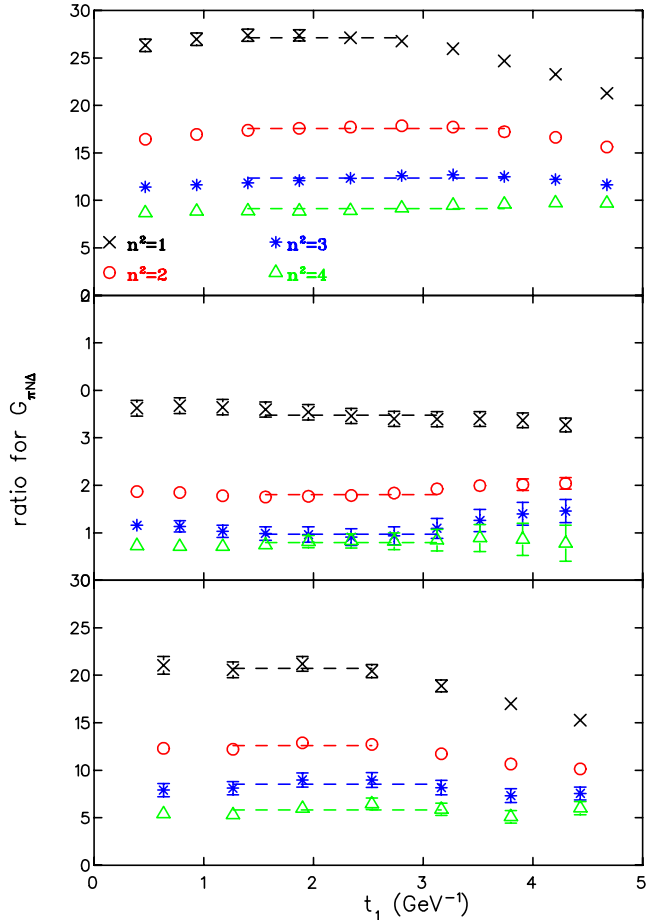

FIG. 4 (color online). The ratio $R^P_{N\Delta}$ used to extract $G_{\pi N\Delta}$ for the four lowest values of Q^2. The upper graph is for the quenched theory, the middle graph for dynamical Wilson fermions, and the lower graph for the hybrid scheme for a pion of mass about 500 MeV (intermediate value). The dashed lines are fits to the plateaus and span the range of fitted points.

constant within the plateau range with a χ^2/degrees of freedom(d.o.f) $\lesssim 1$ to extract the $\pi N\Delta$ form factor.

In Fig. 5 we show the ratio R^A defined in Eq. (19) for the optimal combination that, for large t_1 and $t_2 - t_1$ time intervals, leads to Eq. (21). We show results for the four lowest values of the lattice momentum vector, $\mathbf{q}$, since, in this case, the ratio depends on the momentum vector and not just its magnitude. We note that this is not what is actually fitted, since in our overconstrained analysis we consider all lattice vectors $\mathbf{q}$ that result in the same Q^2 value. However Fig. 5 gives an idea of the quality of the plateaus that are used in the overconstrained analysis to extract the nucleon axial form factors. Similar plateaus are obtained for the ratio $R^A_{N\Delta}$ needed to extract the N to Δ axial form factors. Again the quality of the data allows

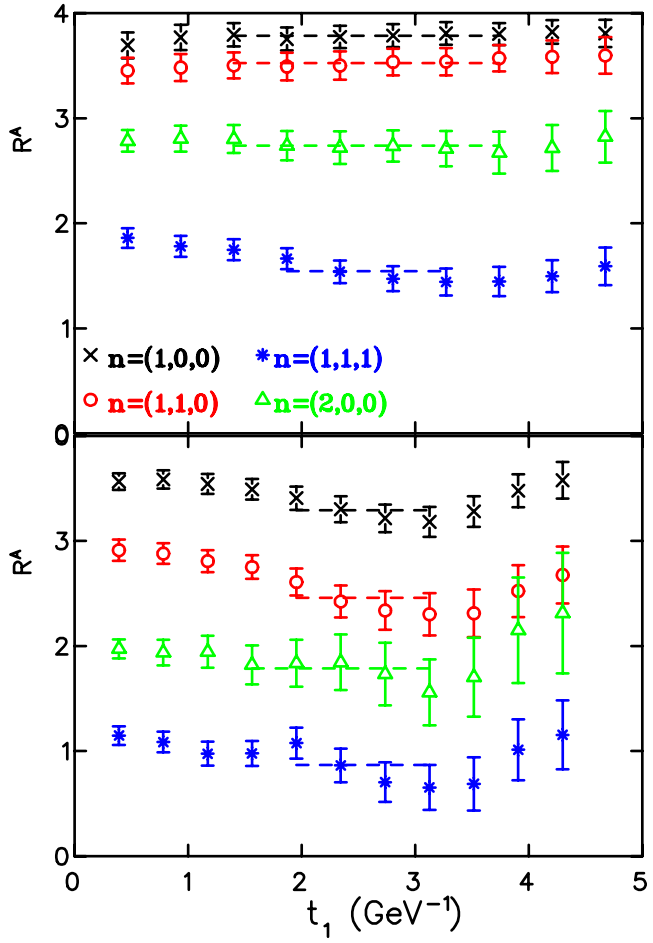

FIG. 5 (color online). The ratio R^A defined in Eq. (19) with the optimal nucleon sink S^A from which G_A and G_p are extracted for the four lowest momentum vectors $\mathbf{q} = (1,0,0)2\pi/L_s$, $\mathbf{q} = (1,1,0)2\pi/L_s$, $\mathbf{q} = (1,1,1)2\pi/L_s$, and $\mathbf{q} = (2,0,0)2\pi/L_s$, where L_s is the spatial size of the lattice. The upper graph is for the quenched theory at intermediate pion mass ($\kappa = 0.1558$) and the lower for two dynamical Wilson quarks at the heaviest mass ($\kappa = 0.1575$). The dashed lines are fits to the plateaus and span the range of fitted points.

identification of a plateau region to which to perform a fit to a constant to extract the matrix element we are interested in.

The overconstrained analysis uses all the stochastically independent lattice measurements that contribute at a given Q^2 when extracting the form factors [41]. This is done by solving the overcomplete set of equations

$$P(\mathbf{q};\mu) = D(\mathbf{q};\mu)\cdot F(Q^2), \tag{44}$$

where $P(\mathbf{q};\mu)$ are lattice measurements of appropriately defined ratios. For concreteness, let us consider the analysis for the nucleon axial form factors. In this case $P(\mathbf{q};\mu)$ is the ratio R^A given in Eq. (19) having statistical errors w_k. The vector F contains the form factors:

$$F(Q^2) = \begin{pmatrix} G_A(Q^2) \\ G_p(Q^2) \end{pmatrix}. \tag{45}$$

If N is the number of current directions and momentum vectors contributing to a given Q^2 then D is an $N \times 2$ matrix, which depends on kinematical factors. We extract the form factors by minimizing

$$\chi^2 = \sum_{k=1}^{N} \left(\frac{\sum_{j=1}^{2} D_{kj} F_j - P_k}{w_k} \right)^2 \tag{46}$$

using the singular value decomposition of D. Therefore we do not actually fit to the plateaus shown in Fig. 5 for each momentum vector but combine all momentum vectors in the overconstrained analysis. A similar analysis is done for the determination of all the other form factors.

C. Fixing the source-sink time separation

All the results shown in Figs. 3–5 are obtained keeping the source-sink separation, t_2, fixed. In the quenched case we take $t_2/a = 11$, for dynamical Wilson fermions we take $t_2/a = 12$ and for the hybrid scheme we take $t_2/a = 8$ so as to keep the physical time separation approximately constant at about 5 GeV^{-1} or 1 fm. In order to ensure that this time separation is large enough to isolate the nucleon and Δ states we must increase the sink-source time separation and check that the results remain unchanged. This check is carried out in the quenched theory at the lowest quark mass and in the hybrid scheme. In both, we increase the source-sink separation by two time slices.

We choose to do this check for quenched rather than dynamical Wilson fermions since the errors are smaller and we can therefore identify deviations more easily. We choose the smallest mass to be as close as possible to the physical limit. In Fig. 6 we show the ratio R^A for the optimal nucleon source S^A of Eq. (21) for source-sink time separation $t_2/a = 11$ and $t_2/a = 13$. Results are shown for the lowest momentum vector $\mathbf{q} = (1,0,0)2\pi/L_s$ and for $\mathbf{q} = (1,1,1)2\pi/L_s$, where L_s is the spatial extent of the lattice. As can be seen the ratios yield consistent plateaus. In the same figure we also show

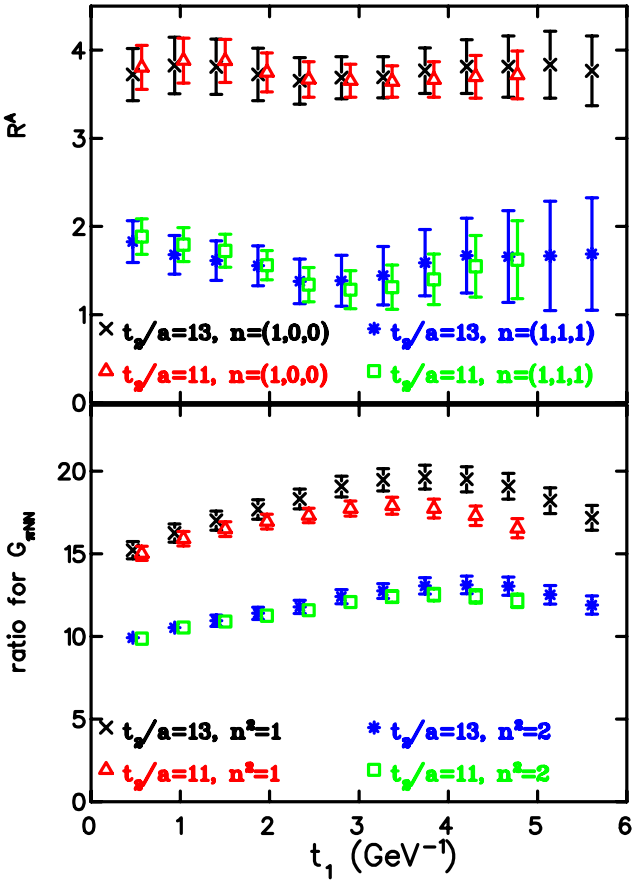

FIG. 6 (color online). The upper graph shows R^A, from which G_A and G_p are extracted, for momentum vectors $\mathbf{q} = (1,0,0)2\pi/L_s$ and $\mathbf{q} = (1,1,1)2\pi/L_s$. The lower graph shows the ratio R^P, from which $G_{\pi NN}$ is determined, for momentum transfer squared $\mathbf{q}^2 = (2\pi/L_s)^2$ and $\mathbf{q}^2 = 2(2\pi/L_s)^2$. Results on these quantities are shown as a function of t_1 for the quenched theory for sink-source separations, $t_2/a = 13$ (crosses and asterisks), and $t_2/a = 11$ (open triangles and squares) at the smallest quark mass ($\kappa = 0.1562$).

the ratio R^P from which $G_{\pi NN}$ is extracted for the two lowest $\mathbf{q}^2$-values. The only discrepancy arises at the lowest $\mathbf{q}^2$ value, where the larger source-sink separation produces a larger result. At all higher values of $\mathbf{q}^2$, the plateaus are however consistent as demonstrated for the second lowest value of $\mathbf{q}^2$. Given that the plateaus for R^A for both time separations are consistent at all values of the momentum vectors, the discrepancy seen in the case of R^P at the smallest $\mathbf{q}^2$ value may have a different origin. We note that S^P is proportional to $q_1 + q_2 + q_3$. As $\mathbf{q} \to 0$ extracting $G_{\pi NN}$ becomes ill-defined and our statistical error in this case underestimates the true error. The effect of increasing t_2 on the actual form factors can be seen in Fig. 7, where we show the nucleon axial form factors $G_A(Q^2)$ and $G_p(Q^2)$ as well as $G_{\pi NN}(Q^2)$ extracted for sink-source separations $t_2/a = 11$ and $t_2/a = 13$. As can be seen, the results up to $Q^2 \sim 1.5$ GeV^2 at the two time separations are within error bars with the only exception the value of $G_{\pi NN}$ at the lowest Q^2 value, which differs by about 1 standard deviation. Differences by about 1 standard deviation in the results for $G_A(Q^2)$ for $Q^2 > 1.5$ GeV^2 are, most likely, due to taking numerically the Fourier transform, which for large values of Q^2, becomes noisy, requiring more statistics. Given this level of agreement at the smallest quark mass we conclude that, for the quenched case, a physical time distance of about 5 GeV$^{-1} \sim 1$ fm is sufficient for ground state dominance and identification of a consistent plateau region with the hindsight that $G_{\pi NN}$ at the smallest Q^2 maybe underestimated by about 1 standard deviation.

We next discuss the adequacy of the sink-source separation in the hybrid approach. Pion cloud contributions are expected to become important for dynamical quarks as the quark mass decreases and one must allow a large enough time separation for the pion cloud to develop. Therefore it is important to ensure that the time separation t_2 is large enough for dynamical quarks with the smallest mass. The results for the larger time separation are obtained using

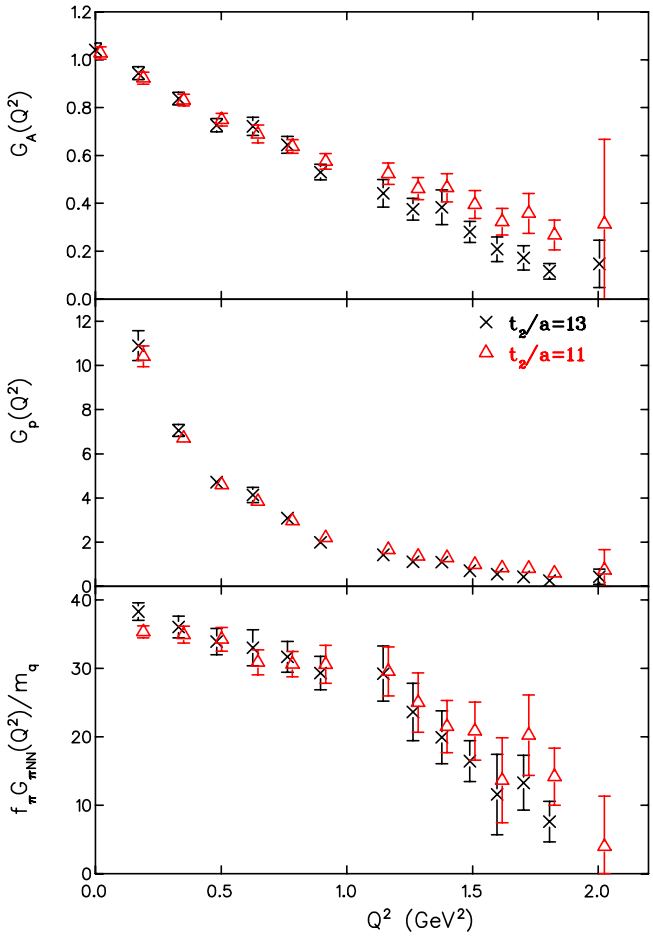

FIG. 7 (color online). The upper graph shows $G^A(Q^2)$, the middle graph $G_p(Q^2)$, and the lower graph $f_\pi G_{\pi NN}/m_q$ as a function of Q^2 in the quenched theory for sink-source separations, $t_2/a = 13$ (crosses), and $t_2/a = 11$ (open triangles) at the smallest quark mass ($\kappa = 0.1562$).

Dirichlet b.c. at the first time slice and at the midpoint of the temporal direction cutting in half the lattice size whereas for the smaller separation antiperiodic b.c. are used. We compare in Fig. 8 the N to Δ form factors extracted for $t_2/a = 10$ to those obtained with sink-source time separation $t_2/a = 8$. As can be seen all the results at the two time separations, including $G_{\pi N\Delta}$ at the lowest $\mathbf{q}^2$ value, are within error bars. Given that we use the same number of configurations for the two time separations it is obvious that we have a big advantage for using the smaller separation since errors are reduced by more that a factor of 2. Given the level of agreement at the smallest quark mass for both quenched and hybrid results, combined with the advantage of smaller statistical errors, we conclude that it suffices to take $t_2 \sim 5$ GeV^{-1}. Therefore all the results given in the next section are obtained with this time separation. Furthermore results in the hybrid scheme are obtained using the full temporal extent of the MILC lattices with antiperiodic b.c. in the temporal direction.

D. Volume dependence

Another potential source of a systematic error is the spatial size of our lattices. Given that for the quenched case we use a lattice of spatial size of about 3 fm we expect finite volume effects to be negligible. A rule of thumb is that finite volume effects are small if $L_s m_\pi \gtrsim 4$–5. For all quark masses used in this work we have $L_s m_\pi > 4.6$, except for dynamical Wilson fermions at the smallest quark mass where we have $L_s m_\pi = 3.6$. Since we do not have dynamical Wilson configurations on a larger volume we test for finite size effects in the hybrid scheme for which, at the smallest quark mass, there are MILC configurations for $L_s = 2.5$ and $L_s = 3.5$ giving $L_s m_\pi = 4.6$ and $L_s m_\pi = 6.4$, respectively. In Fig. 9 we show results for the N to Δ axial form factors $C_5^A(Q^2)$ and $C_6^A(Q^2)$ as well as $G_{\pi N\Delta}(Q^2)$ for these two spatial sizes. Results on the smaller lattice are consistent with results on the larger lattice. This indeed shows that finite volume effects are small for $L_s m_\pi \gtrsim 4.5$. Since for all our quark masses, except the lightest mass in the case of dynamical Wilson

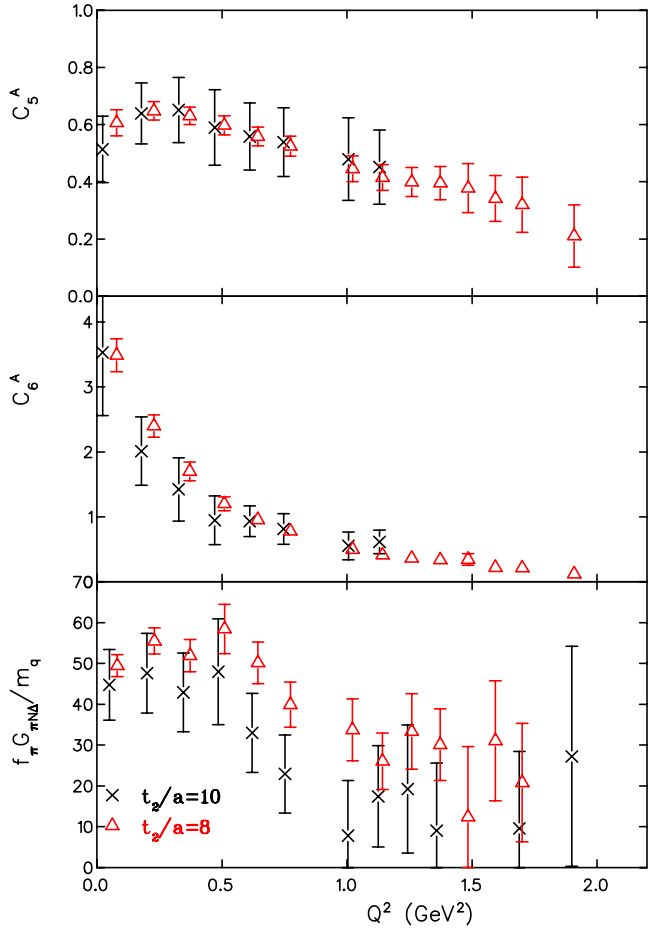

FIG. 8 (color online). The upper graph shows $C_5^A(Q^2)$, the middle graph $C_6^A(Q^2)$, and the lower graph $f_\pi G_{\pi N\Delta}/m_q$ as a function of Q^2 in the hybrid scheme for sink-source separations, $t_2/a = 10$ (crosses), and $t_2/a = 8$ (open triangles) at the smallest quark mass, namely $m_l = 0.01$.

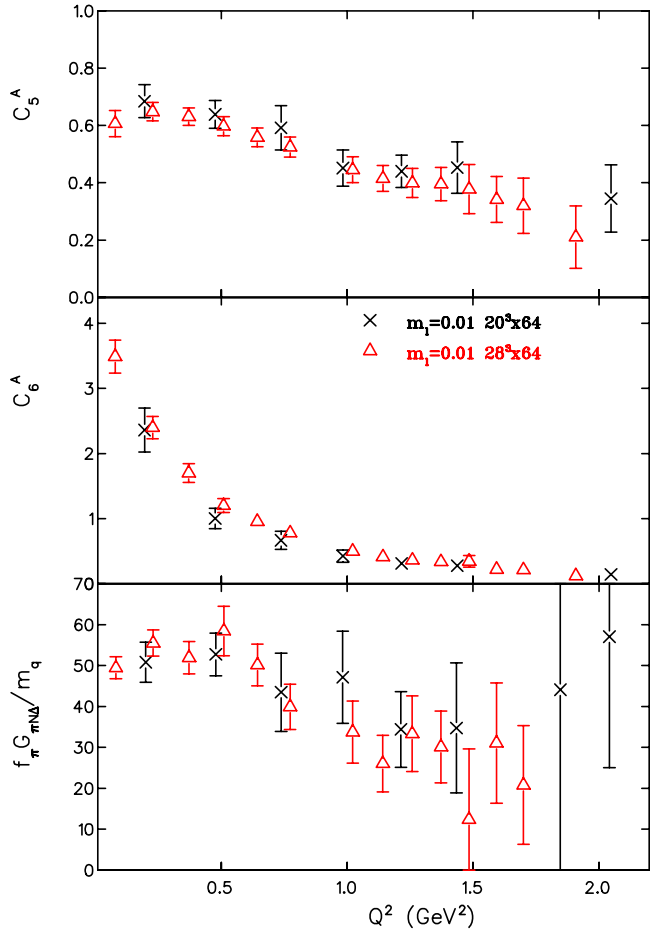

FIG. 9 (color online). The upper graph shows C_5^A, the middle graph C_6^A, and the lower graph $G_{\pi N\Delta}$ as a function of Q^2 in the hybrid approach for spatial volumes, 20^3 with 100 configurations (crosses) and 28^3 with 150 configurations (open triangles) at the smallest quark mass, $m_l = 0.01$.

fermions, $L_s m_\pi > 4.6$, we expect finite volume effects to be small. We note, however, that a systematic study of volume effects that would allow an extrapolation of our quantities to infinite volume requires results using at least three different volumes. This is beyond the scope of the present work.

Finally we comment on the evaluation of the kinematical factors in the expressions for the form factors, which involve the masses of the nucleon and Δ and their energies. The masses are evaluated using two-point functions in the standard way. The energies are calculated using the continuum dispersion relation, $E = \sqrt{m^2 + p^2}$, where $p^2 = n(2\pi/L_s)^2$, $n = 1, 2, \ldots$. One can compare results obtained using continuum dispersion relations to those obtained with the lattice dispersion relation $\sinh^2(E) = \sinh^2 m + \sum_{i=1,\ldots,3} \sin^2 2\pi n_i/L_s$. We find that the mean value of the form factors is almost unchanged. The Q^2-values are also very close for $Q^2 \lesssim 1$ GeV^2. At larger momentum transfers the lattice dispersion relation shifts the Q^2 to smaller values. Using two-point functions to extract the energy also yields consistent results for the form factors albeit with larger errors. In what follows we will present results as a function of Q^2 calculated using the continuum dispersion relation.

V. RESULTS

We first discuss results on quantities and ratios for which the renormalized quark mass is not required. This eliminates one source of systematic error, namely, lattice artifacts on the value of m_q. Furthermore, in general, ratios show weaker dependence on quark mass. For these reasons, they are more suited for comparison with physical results.

For the same lattice momentum vectors the Q^2 values for the nucleon system differ from those in the $N - \Delta$ system. In order to take ratios of form factors computed in these two different systems we interpolate the form factors in the nucleon system to the Q^2 value of the $N - \Delta$ system. In Fig. 10 we show the ratio of the form factors $G_{\pi N\Delta}(Q^2)/G_{\pi NN}(Q^2)$ for quenched and two degenerate flavors of dynamical Wilson quarks denoted by $N_F = 0$ and $N_F = 2$ respectively. As can be seen, this ratio is Q^2 independent and shows no statistically significant quark mass dependence. Fitting the quenched results to a constant we obtain the value of 1.60(2) shown by the dashed line. The unquenched results are more noisy and a fit to a constant yields a ratio of 1.63(4), which is consistent with the quenched result. If we assume pion pole dominance for the form factors $G_p(Q^2)$ and $C_6^A(Q^2)$ then the GTRs simplify to the relations given in Eq. (14). Taking the ratio of the diagonal and nondiagonal relations we find that $G_{\pi N\Delta}(Q^2)/G_{\pi NN}(Q^2) = 2C_5^A(Q^2)/G_A(Q^2)$. In Fig. 11, we show the ratio $2C_5^A(Q^2)/G_A(Q^2)$, which is indeed also Q^2 independent, and fitting to the quenched data we find the value of 1.63(1) shown by the dashed line. The unquenched data lie higher than quenched and a fit yields a value of 1.75(3). Therefore, on the level of ratios, the GTRs are satisfied in the quenched case where the results are most accurate. In the unquenched case they differ by about 2 standard deviations. We can use the relations given in Eq. (13) for G_p and C_6^A to eliminate $G_{\pi NN}$ and $G_{\pi N\Delta}$ in Eqs. (11) and (12) to obtain

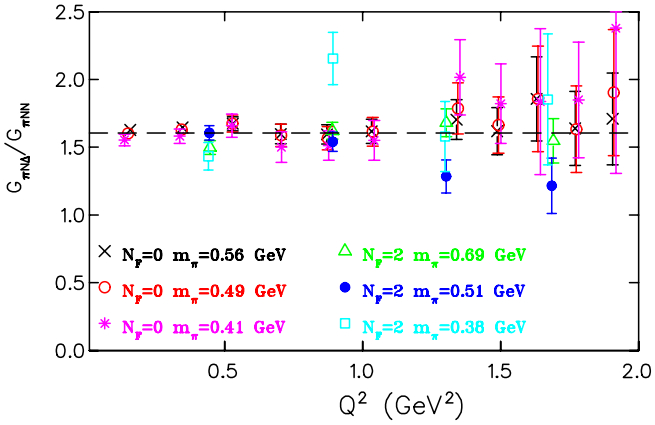

FIG. 10 (color online). The ratio of form factors $G_{\pi N\Delta}(Q^2)/G_{\pi NN}(Q^2)$ as a function of Q^2 for Wilson fermions for the quenched theory, denoted by $N_F = 0$, at $\kappa = 0.1554(m_\pi = 0.56$ GeV), $\kappa = 0.1558(m_\pi = 0.49$ GeV), and $\kappa = 0.1562(m_\pi = 0.41$ GeV) and for two dynamical Wilson quarks, denoted by $N_F = 2$, at $\kappa = 0.1575(m_\pi = 0.69$ GeV) [30], $\kappa = 0.1580(m_\pi = 0.51$ GeV) [30], and $\kappa = 0.158\,25(m_\pi = 0.38$ GeV) [31]. The dashed line is the result of fitting the quenched results to a constant, yielding a value of 1.60(2).

$$G_p(Q^2) = \frac{4m_N^2/m_\pi^2}{1 + Q^2/m_\pi^2} G_A(Q^2),$$
$$C_6^A(Q^2) = \frac{m_N^2/m_\pi^2}{1 + Q^2/m_\pi^2} C_5^A(Q^2). \quad (47)$$

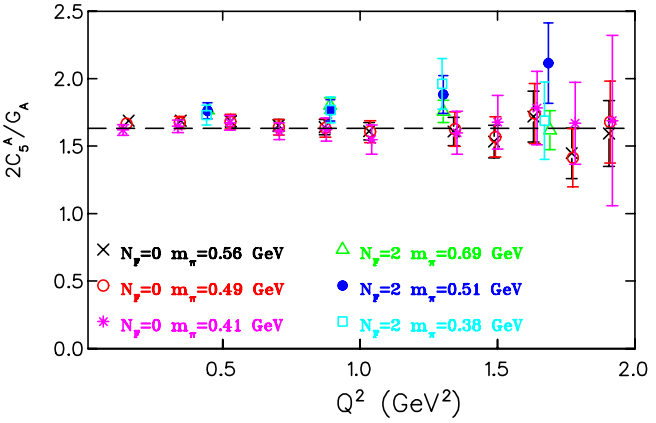

FIG. 11 (color online). The ratio of $2C_5^A(Q^2)/G_A(Q^2)$ as a function of Q^2. The notation is the same as that of Fig. 10. Fitting the quenched results to a constant yields a value of 1.63(1).

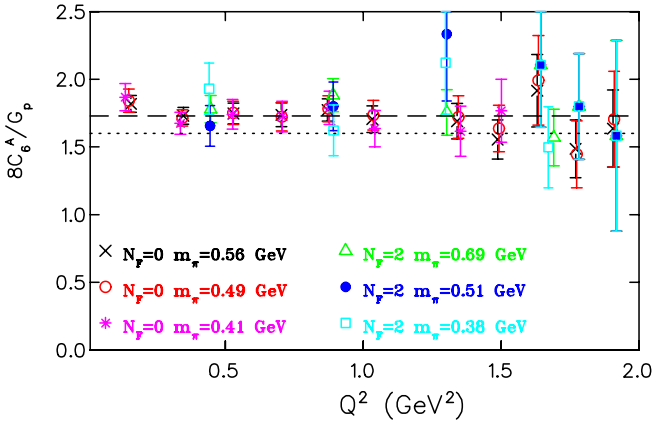

FIG. 12 (color online). The ratio of $8C_6^A(Q^2)/G_p(Q^2)$ as a function of Q^2. The notation is the same as that of Fig. 10. Fitting the quenched results to a constant yields a value of 1.73(3). The dotted line denotes the value of 1.60 obtained by fitting the ratio $G_{\pi N\Delta}(Q^2)/G_{\pi NN}(Q^2)$.

These relations are again a manifestation of pion pole dominance. Taking ratios, we find that $8C_6^A(Q^2)/G_p(Q^2)$ should be equal to the ratio $2C_5^A(Q^2)/G_A(Q^2)$ and consequently to $G_{\pi N\Delta}(Q^2)/G_{\pi NN}(Q^2)$. As can be seen in Fig. 12, we indeed find that also this ratio is constant as a function of Q^2. Fitting the quenched data to a constant we obtain the value of 1.73(3), shown by the dashed line in the figure. This is about 6% larger than what we find for the other two ratios. Fitting the unquenched data we find $8C_6^A(Q^2)/G_p(Q^2) = 1.78(5)$ consistent with the quenched result and higher than the ratio $G_{\pi N\Delta}(Q^2)/G_{\pi NN}(Q^2)$. Therefore we conclude that ratios based on the relations given in Eqs. (14) and (47) are satisfied on the few percent level. Relaxing the assumption on pion pole dominance of G_p and C_6^A, we can consider directly the ratio of the non-diagonal to the diagonal GTR given in Eqs. (11) and (12) respectively. As can be seen in Fig. 13, the ratio is indeed consistent with unity.

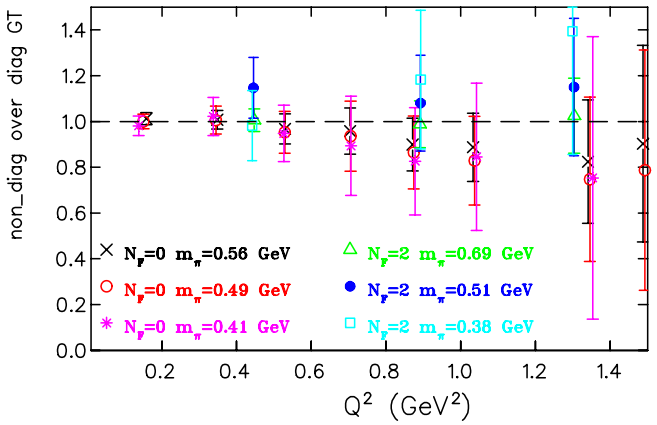

FIG. 13 (color online). The ratio of Eq. (12) to Eq. (11). The notation is the same as that of Fig. 10.

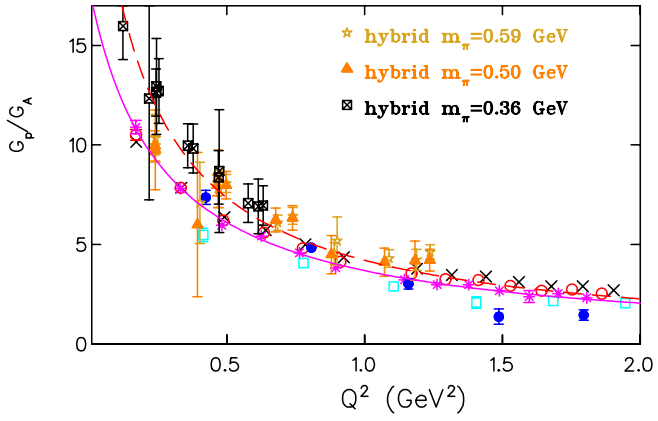

FIG. 14 (color online). The ratio of nucleon axial form factors $G_p(Q^2)/G_A(Q^2)$ for Wilson fermions for the quenched theory and for two dynamical Wilson quarks using the same notation as in Fig. 10. We also show results from Ref. [27] obtained in the hybrid approach using the same quark masses as the ones used in this work, namely $m_l = 0.03$ (stars), $m_l = 0.02$ (filled triangles), and $m_l = 0.01$ (inscribed squares). The dashed line shows the expected behavior assuming pion pole dominance as given in Eq. (47), where for m_π and m_N we use the values computed on the lattice at $\kappa = 0.1562$. The solid curve is a fit to a monopole form of the quenched data at $\kappa = 0.1562$.

Having examined the Q^2-dependence on the level of ratios of GTRs in the nucleon and $N-\Delta$ systems we now discuss the Q^2 dependence of the form factors for the two systems separately. In Fig. 14 we show the ratio of nucleon axial form factors $G_p(Q^2)/G_A(Q^2)$ as a function of Q^2 for quenched and two degenerate flavors of dynamical Wilson quarks. Recent results from Ref. [27] obtained in the hybrid scheme at the same quark masses as the ones used in this work for the calculation of the N to Δ form factors are also included. In all cases, the ratio decreases with Q^2 confirming the stronger Q^2-dependence expected

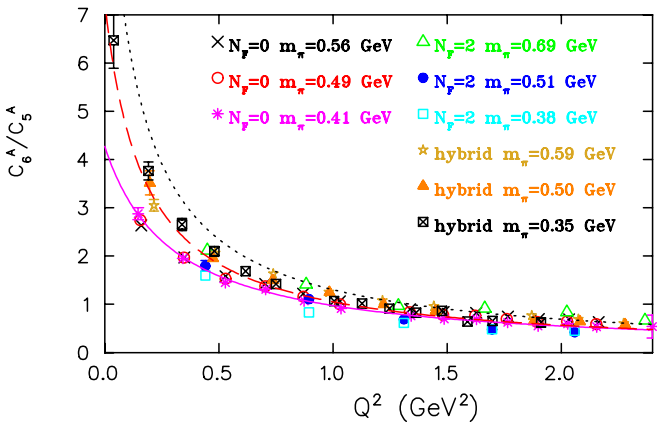

FIG. 15 (color online). The ratio of N to Δ axial transition form factors $C_6^A(Q^2)/C_5^A(Q^2)$. The notation is the same as that of Fig. 14. The dotted line shows the prediction of pion pole dominance predicted in Eq. (47) but for the hybrid case at the lightest quark mass.

for $G_p(Q^2)$ as compared to $G_A(Q^2)$. A similar behavior is also observed for the corresponding ratio $C_6^A(Q^2)/C_5^A(Q^2)$ for N to Δ shown in Fig. 15. If pion pole dominance holds, then the ratios $G_p(Q^2)/G_A(Q^2)$ and $C_6^A(Q^2)/C_5^A(Q^2)$ should be described by the relations given in Eq. (47) with no adjustable parameters. In Figs. 14 and 15 we show, with the dashed lines, the resulting curves for the case of quenched lattice results at the lightest pion mass obtained assuming the relations given in Eqs. (47). As can be seen, as $Q^2 \to 0$, both ratios increase slower than pion pole dominance predicts. In addition we show by the solid curves fits to the same quenched data using a monopole form

$$\frac{c_0}{(Q^2/m^2 + 1)} \tag{48}$$

with fit parameters c_0 and m. The values of c_0 and m extracted from the fits are given in Table III. In the quenched case, we find that $m > m_\pi$, whereas for the hybrid scheme, although $m \sim m_\pi$, c_0 is smaller than m_N^2/m_π^2 causing the dotted line shown in Fig. 15, obtained at the lightest quark mass, to be higher than the corresponding lattice results. The calculation in the hybrid scheme at the lightest quark mass is done on a larger lattice enabling us to compute the form factors at low Q^2-values, much lower than in the case of dynamical Wilson fermions. These results show clear deviations from quenched results at low Q^2, where pion clouds effects are expected to dominate.

In order to examine the Q^2-dependence of the form factors separately and compare with continuum quantities, we need to multiply lattice results with the axial renormalization constant Z_A. These constants are known for both Wilson fermions and DWF within the hybrid scheme. The values that we use are given in Table IV. We collect our lattice results for the nucleon form factors in Tables V and VI and for N to Δ in Tables VII, VIII, and IX of the Appendix. All errors are calculated using jackknife analysis. In Fig. 16, we show $G_A(Q^2)$ and the induced pseudoscalar form factor $G_p(Q^2)$. For comparison we also show results obtained in the hybrid approach from Ref. [27]. The main observation is again that at the smallest domain wall quark mass, the hybrid results show deviations. In particular, we note that the value for the nucleon axial charge g_A

TABLE III. The first column gives the pion mass in GeV, the second and third columns the fit parameters m and c_0 extracted from fitting the ratio G_p/G_A (C_6^A/C_5^A) for the nucleon (N to Δ) case, the fourth and fifth columns the dipole parameters m_A and g_0 extracted from fitting G_A (C_5^A) for the nucleon (N to Δ), and the sixth and seventh columns the corresponding parameters but using an exponential Ansatz $\tilde{g}_0 \exp(-Q^2/\tilde{m}_A^2)$. The eighth column gives Δ or Δ' defined in Eq. (52). The last two columns give the value of the strong coupling constants $g_{\pi NN}$ or $g_{\pi N\Delta}$. The first value of the strong coupling constant is determined using the fit function of Eq. (53), the second using a linear fit according to Eq. (52).

Nucleon elastic									
m_π (GeV)	m (GeV)	c_0	m_A (GeV)	g_0	$\tilde{m}_A$ (GeV)	$\tilde{g}_0$	Δ	$g_{\pi NN}$	
Quenched Wilson fermions									
0.563(4)	0.671(14)	13.71(34)	1.659(20)	1.088(8)	1.271(9)	1.074(5)	0.110(2)	9.943(99)	10.609(73)
0.490(4)	0.597(14)	15.23(43)	1.632(19)	1.079(7)	1.249(9)	1.069(5)	0.083(2)	9.126(93)	10.143(91)
0.411(4)	0.511(16)	17.70(76)	1.578(28)	1.080(12)	1.220(10)	1.066(6)	0.062(2)	8.410(100)	9.725(140)
$N_F = 2$ dynamical Wilson fermions									
0.691(8)	0.750(43)	14.13(1.01)	1.831(22)	1.067(6)	1.393(16)	1.063(6)	0.114(3)	11.48(245)	10.486(122)
0.509(8)			1.709(46)	0.999(17)	1.296(29)	0.995(17)	0.038(15)		9.071(294)
0.384(8)	0.642(77)	11.15(1.82)	2.019(78)	0.951(18)	1.528(44)	0.943(15)	0.044(10)		8.613(551)
Nucleon to Δ									
m_π (GeV)	m (GeV)	c_0	m_A (GeV)	g_0	$\tilde{m}_A$ (GeV)	$\tilde{g}_0$	Δ'	$g_{\pi N\Delta}$	
Wilson fermions quenched									
0.563(4)	0.691(13)	3.44(79)	1.544(32)	0.952(16)	1.205(8)	0.926(5)	0.106(2)	16.560(194)	17.174(166)
0.490(4)	0.624(15)	3.75(12)	1.537(33)	0.930(14)	1.192(10)	0.910(7)	0.079(2)	14.692(188)	16.195(206)
0.411(4)	0.545(16)	4.23(17)	1.534(36)	0.906(15)	1.189(13)	0.887(9)	0.052(2)	12.609(180)	14.873(264)
Wilson fermions, dynamical $N_F = 2$									
0.691(8)	0.604(95)	4.75(1.04)	1.696(51)	0.988(24)	1.368(13)	0.937(5)	0.109(2)		17.536(190)
0.509(8)	0.352(151)	8.38(6.11)	1.760(59)	0.865(25)	1.454(46)	0.808(20)	0.063(2)		14.970(452)
0.384(8)	0.379(58)	6.34(1.69)	1.968(118)	0.843(40)	1.410(51)	0.808(24)	0.024(15)		12.685(1.416)
Hybrid action									
0.594(1)	0.576(28)	5.08(22)	1.924(85)	0.883(22)	1.477(42)	0.868(15)	0.076(5)		17.649(236)
0.498(3)	0.485(27)	6.15(52)	1.892(101)	0.864(32)	1.505(71)	0.835(27)	0.0648(7)		17.329(496)
0.353(3)	0.384(15)	8.64(55)	2.202(113)	0.750(19)	1.666(65)	0.741(15)	0.036(5)	12.282(289)	13.472(487)

TABLE IV. The first column gives the hopping parameter κ for Wilson fermions or the mass of the domain wall fermion, the second the renormalized quark mass, the third the unrenormalized pion decay constant f_π/Z_A in lattice units, and the fourth the axial renormalization constant Z_A.

κ or m_l	am_q	af_π/Z_A	Z_A
Quenched Wilson fermions			
0.1554	0.0403(4)	0.0611(14)	0.808(7) [42]
0.1558	0.0307(4)	0.0587(16)	0.808(7)
0.1562	0.0213(4)	0.0563(17)	0.808(7)
$N_F = 2$ Wilson fermions			
0.1575	0.0441(4)	0.0649(8)	0.77(2) [43]
0.1580	0.0229(4)	0.0494(9)	0.78(4) [43]
0.15825	0.0122(3)	0.0467(13)	0.8[a]
Hybrid action			
0.03	0.0475(3)	0.0678(6)	1.1085(5) [23]
0.02	0.0324(4)	0.0648(8)	1.0994(4) [23]
0.01	0.0157(2)	0.0639(2)	1.0847(6) [23]

[a]Estimated from the values of Z_A at $\kappa = 0.1575$ and 0.1580.

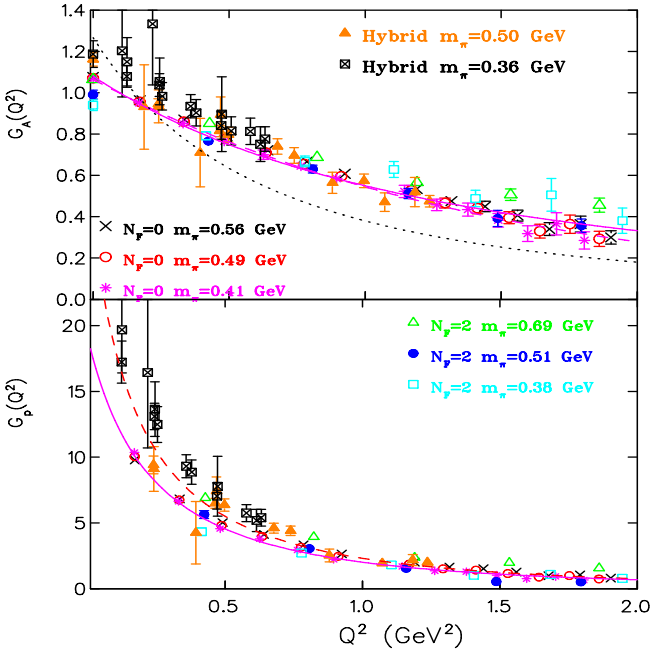

FIG. 16 (color online). The upper graph shows $G_A(Q^2)$ and the lower graph $G_p(Q^2)$ as a function of Q^2. The solid curve is a fit to a dipole form of the quenched results at $\kappa = 0.1562$. The fit to an exponential form shown by the dashed line falls on top. The dotted line shown in the upper graph corresponds to a dipole form with axial mass $m_A = 1.1$ GeV used to describe experimental data. The dashed line in the lower graph shows the result expected from pion pole dominance in Eq. (47). The solid line corresponds to Eq. (50). The rest of the notation is the same as that in Fig. 14. Results in the hybrid approach are from Ref. [27].

becomes larger in the hybrid scheme approaching the experimental value. This is in agreement with the findings of Ref. [23]. Since there are recent state-of-the-art lattice studies of g_A [23,24] we will not discuss it further here but rather investigate the Q^2 dependence of the form factors. We also find that $G_p(Q^2)$ increases more rapidly at low Q^2 in the hybrid scheme when the pion mass decreases to about 350 MeV. In Fig. 17 we show the corresponding N to Δ transition form factors $C_5^A(Q^2)$ and $C_6^A(Q^2)$. The hybrid results show the same behavior as in the case of the nucleon form factors, yielding a different behavior at low Q^2 when the pion mass becomes about 350 MeV. The Q^2-dependence of both $G_A(Q^2)$ and $C_5^A(Q^2)$ can be well described by a dipole Ansatz

$$\frac{g_0}{(Q^2/m_A^2 + 1)^2}. \tag{49}$$

This is what is usually used to describe experimental data for $G_A(Q^2)$ where a value of $m_A \sim 1.1$ GeV is extracted for the axial mass. The same dipole Ansatz is also used to describe $C_5^A(Q^2)$, where an axial mass of 1.28 ± 0.10 GeV [44] has been found. In addition, we fit to an exponential form given by $\tilde{g}_0 e^{-Q^2/\tilde{m}_A^2}$. Both Ansätze describe well our results as can be seen in Figs. 16 and 17 where the two lines, which are fits to quenched lattice results at the smallest quark mass, can hardly be distinguished. The values of the axial masses extracted from these fits are given in Table III. We find an axial mass that is larger than what is deduced from experiment. This means that $G_A(Q^2)$ and $C_5^A(Q^2)$ fall off slower than in experiment. This is clearly seen in Fig. 16 where we include the dipole curve taking $m_A = 1.1$ GeV. Having fitted $G_A(Q^2)$ and $C_5^A(Q^2)$, the Q^2-dependence for the form factors $G_p(Q^2)$ and $C_6^A(Q^2)$ can be obtained using Eq. (47). The resulting curves are shown by the dashed line in Figs. 16 and 17 and show deviations at low Q^2. In addition we show curves that correspond to

$$\frac{g_0 c_0}{(Q^2/m_A^2 + 1)^2 (Q^2/m^2 + 1)} \tag{50}$$

with m extracted from fitting the ratio of $G_p(Q^2)/G_A(Q^2)$ in the case of the nucleon system and $C_6^A(Q^2)/C_5^A(Q^2)$ for the N to Δ. As expected this provides a good description of the Q^2-dependence for both $G_p(Q^2)$ and $C_6^A(Q^2)$ shown by the solid lines, which correspond to the parameters of the quenched data at $\kappa = 0.1562$.

We now present results that require knowledge of the renormalized quark mass. The renormalized quark mass, m_q, is determined by evaluating the pion to vacuum matrix element of the axial Ward-Takahashi identity given in Eq. (8). As mentioned already, for Wilson fermions the axial Ward identity is satisfied only up to $\mathcal{O}(a)$ terms. We expect these corrections to become more severe as we approach the chiral limit. As we already mentioned, the quark mass in the hybrid scheme, m_q^{DW}, was tuned to reproduce the mass of the lightest pion in the staggered theory. Given that domain wall fermions satisfy the AWI when the size of the fifth dimension is taken to infinity,

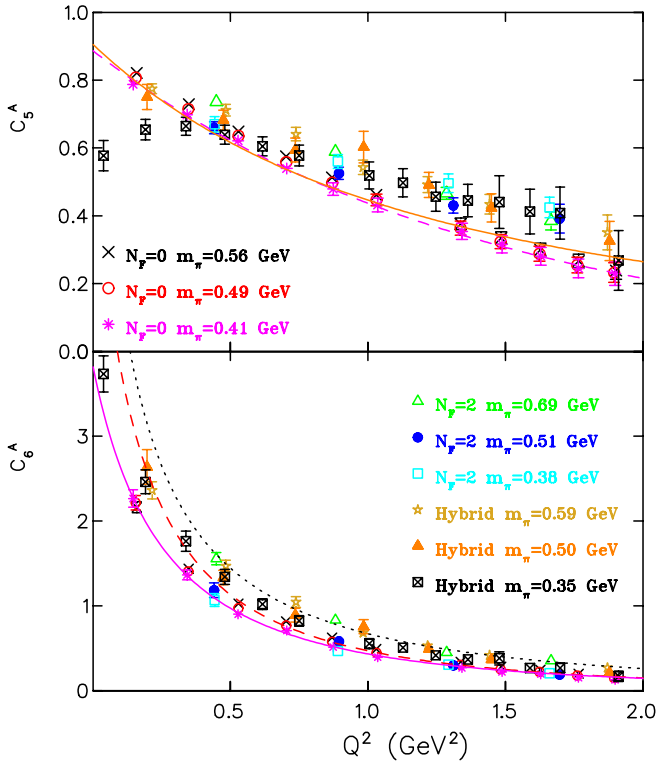

FIG. 17 (color online). The upper graph shows $C_5^A(Q^2)$ and lower graph $C_6^A(Q^2)$ as a function of Q^2. The notation is the same as that in Fig. 15.

corrections to Eq. (8) come from the residual mass due the finite length of the fifth direction. Therefore differences between the values of m_q and m_q^{DW} are due to chiral symmetry breaking because of the finite size of the fifth dimension. We show in Fig. 18, the renormalized quark mass extracted from the axial Ward identity for quenched and two dynamical Wilson fermions and in the hybrid approach. As can be seen, the pion mass extrapolates to zero at $m_q = 0$ for the quenched theory. For dynamical Wilson fermions m_π is not exactly zero at $m_q = 0$ indicating finite a-corrections. For the hybrid scheme we show both the renormalized mass computed using the AWI, m_q, and m_q^{DW}. As can be seen m_q is approximately equal to m_q^{DW} confirming that the residual mass is small. The biggest deviation, as expected, is observed at the smallest value of the quark mass. From these results we confirm that in the hybrid scheme $m_\pi^2 \propto m_q$ within our statistical errors.

Having determined m_q and f_π using Eq. (40) we can evaluate the form factors $G_{\pi NN}(Q^2)$ and $G_{\pi N\Delta}(Q^2)$. We first examine the Goldberger-Treiman relations as given in Eq. (14) by considering the ratios $f_\pi G_{\pi NN}(Q^2)/m_N G_A(Q^2)$ and $f_\pi G_{\pi N\Delta}(Q^2)/2m_N C_5^A(Q^2)$, which should be equal to unity. Note that in these ratios the axial and pseudoscalar renormalization constants cancel. These ratios are shown in Fig. 19. We find that, in the quenched theory, they are less than one for small Q^2 but

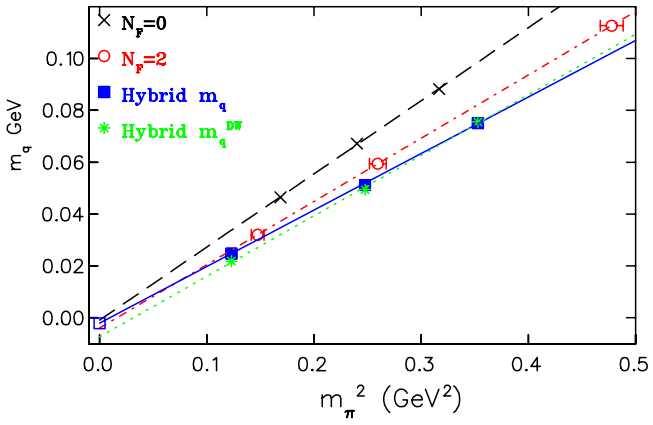

FIG. 18 (color online). The renormalized quark mass m_q versus m_π^2 for the quenched theory (crosses), for two dynamical Wilson fermions (open circles), and for the hybrid scheme (filled squares). In the hybrid case we also show m_q^{DW} (asterisks) determined by tuning the pion mass [37]. The lines are linear fits to m_π^2. The open square shows the extrapolated value of m_q in the hybrid scheme.

become one for $Q^2 \gtrsim 0.5$ GeV^2. This is also approximately true for dynamical Wilson for the two heaviest quark masses. Results in the hybrid approach, on the other hand, show smaller deviations from unity at low Q^2. We also expect that the ratios

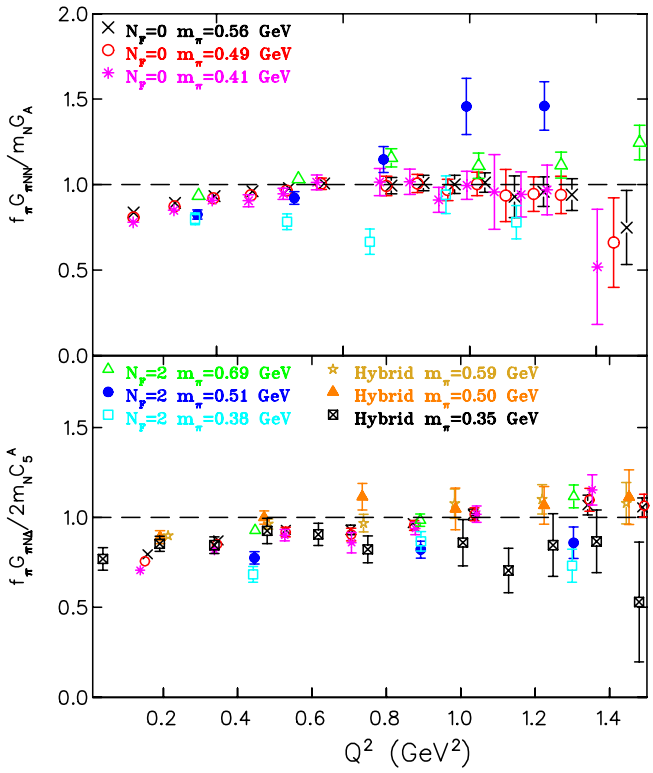

FIG. 19 (color online). The upper graph shows the ratio $f_\pi G_{\pi NN}(Q^2)/m_N G_A(Q^2)$ and the lower graph the ratio $f_\pi G_{\pi N\Delta}(Q^2)/2m_N C_5^A(Q^2)$. The notation is the same as in Fig. 14.

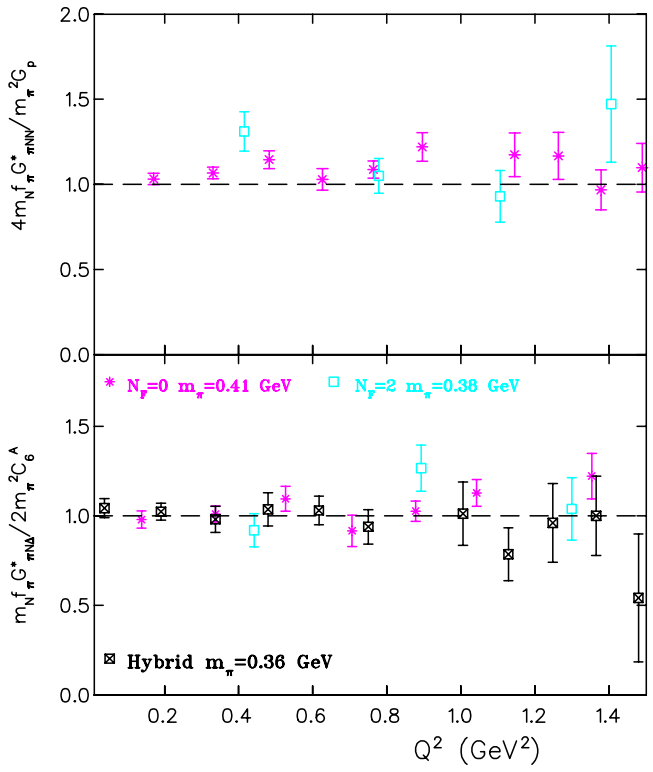

FIG. 20 (color online). The upper graph shows the ratio $4m_N f_\pi G^*_{\pi NN}(Q^2)/m_\pi^2 G_p(Q^2)$ and the lower graph the ratio $m_N f_\pi G^*_{\pi N\Delta}(Q^2)/2m_\pi^2 C_6^A(Q^2)$ for the lightest quark mass considered in each of our three types of calculations. We have defined $G^*_{\pi NN}(Q^2) \equiv G_{\pi NN}(Q^2)/(1 + Q^2/m_\pi^2)$ with a corresponding expression for $G^*_{\pi N\Delta}$.

$$\frac{4m_N f_\pi}{m_\pi^2 G_p(Q^2)} \frac{G_{\pi NN}(Q^2)}{(1 + Q^2/m_\pi^2)}, \qquad \frac{m_N f_\pi}{2m_\pi^2 C_6^A(Q^2)} \frac{G_{\pi N\Delta}(Q^2)}{(1 + Q^2/m_\pi^2)}, \tag{51}$$

should be unity if pion pole dominance is valid. As can be seen in Fig. 20, for the lightest quark masses in our three types of action these ratios are indeed consistent with one.

Finally we discuss the Q^2-dependence of the form factors $G_{\pi NN}(Q^2)$ and $G_{\pi N\Delta}(Q^2)$ separately. In Fig. 21 we show $G_{\pi NN}(Q^2)$ and $G_{\pi N\Delta}(Q^2)$ at the smallest quark mass in the quenched theory and for dynamical Wilson quarks. For $G_{\pi N\Delta}(Q^2)$ we also show results in the hybrid scheme at a similar quark mass. Results for these form factors at small Q^2 are consistent with each other unlike the other form factors, indicating that unquenching effects on these quantities are still small for a pion mass of about 350 MeV. Assuming PCAC and pion pole dominance, the Q^2-dependence of $G_{\pi NN}(Q^2)$ and $G_{\pi N\Delta}(Q^2)$ is completely determined from the GTRs given in Eq. (14) once we know $G_A(Q^2)$ and $C_5^A(Q^2)$. Using the dipole Ansatz of Eq. (49) for the Q^2-dependence of $G_A(Q^2)$ and $C_5^A(Q^2)$ with the parameters given in Table III, we obtain the dashed lines shown in Fig. 21. The discrepancy already observed in the ratio $f_\pi G_{\pi NN}(Q^2)/m_N G_A(Q^2)$ and

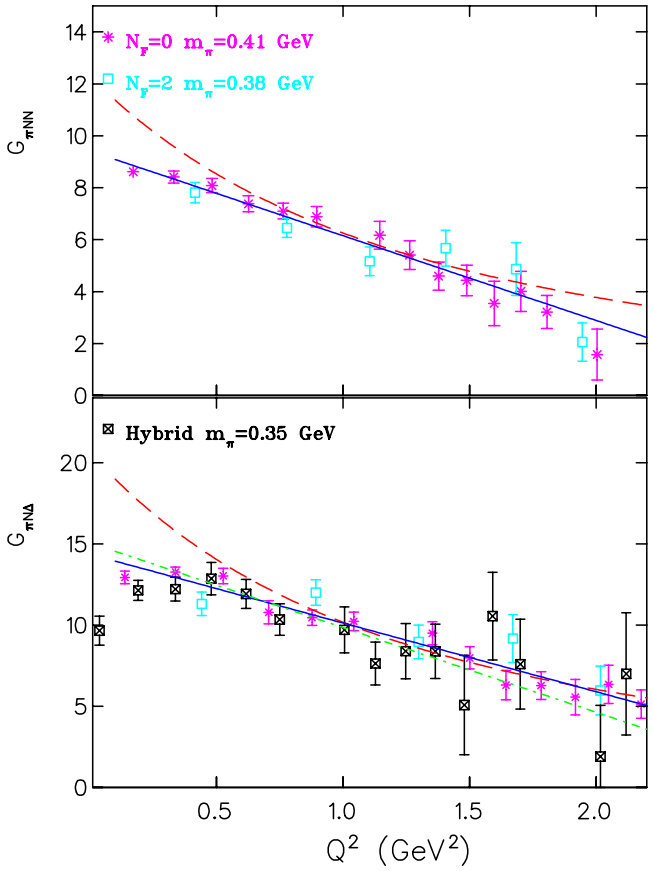

FIG. 21 (color online). The upper graph shows $G_{\pi NN}(Q^2)$ for Wilson fermions at the smallest pion mass. The lower graph shows $G_{\pi N\Delta}(Q^2)$ for Wilson fermions and DWF at the smallest pion mass. The dashed lines follow from the GTR relations given in Eq. (14). The solid lines are fits using Eq. (52). In the case of $G_{\pi N\Delta}(Q^2)$, we also show by the dash-dotted line (with larger slope) the curve that corresponds to taking $G_{\pi N\Delta}(Q^2) = 1.6 G_{\pi NN}(Q^2)$.

$f_\pi G_{\pi N\Delta}(Q^2)/m_N C_5^A(Q^2)$ at low Q^2 values is clearly seen here. Results in the hybrid approach confirm deviations from the GTRs at low Q^2. The Q^2-dependence of $G_{\pi NN}(Q^2)$ and $G_{\pi N\Delta}(Q^2)$ can be described using a linear Ansatz given by

$$\begin{aligned} G_{\pi NN}(Q^2) &= a\left(1 - \Delta \frac{Q^2}{m_\pi^2}\right), \\ G_{\pi N\Delta}(Q^2) &= a'\left(1 - \Delta' \frac{Q^2}{m_\pi^2}\right) \end{aligned} \tag{52}$$

with a (a') and Δ (Δ') fit parameters. These linear fits are shown by the solid curves in Fig. 21 and provide a good description to the results. Note that we have excluded from the fits the value at the lowest Q^2 in all cases in the quenched theory as well as in the hybrid approach at the smallest quark mass, since our statistical error maybe underestimated for this value of Q^2. The values we find for the parameters a (a'), which determine the strong coupling constant $g_{\pi NN}$ ($g_{\pi N\Delta}$), and Δ (Δ') are given in

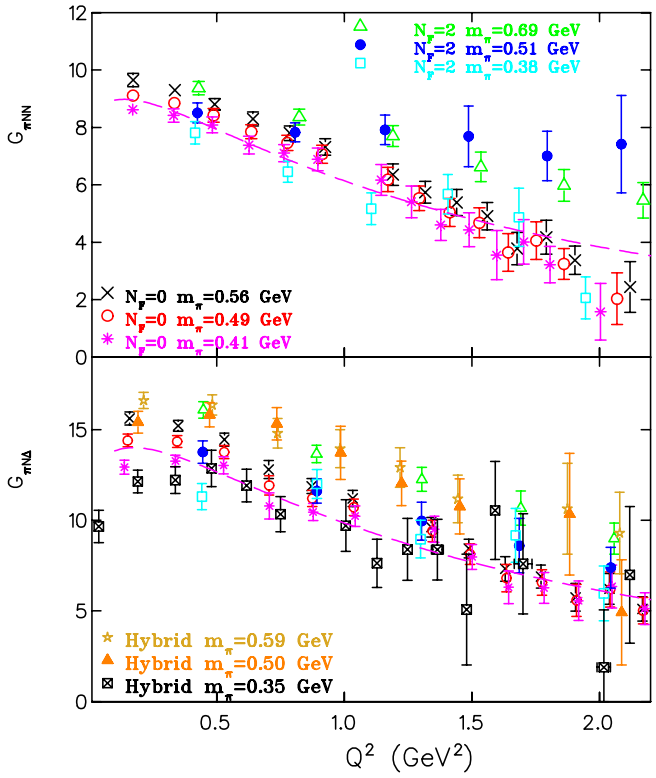

FIG. 22 (color online). The upper graph shows $G_{\pi NN}(Q^2)$ and the lower graph shows $G_{\pi N\Delta}(Q^2)$ as a function of Q^2. The dashed lines are fits to the quenched results at $\kappa = 0.1562$ obtained using the functions of Eq. (53) and allowing an overall constant to be fitted.

Table III. Note that Δ and Δ′ decrease as the quark mass decreases. In the quenched theory at the smallest quark mass $\Delta \sim 6\%$. One expects that this value decreases further as we approach the physical limit becoming comparable to the value of $\Delta = 2.44\%$ obtained using baryon chiral perturbation theory [15]. However, the corresponding value of a is smaller than the expected value of $m_N g_A/f_\pi$ and decreases with the quark mass being about 83% less at the heaviest and about 73% at the lightest quark mass in the quenched theory. The relation $G_{\pi N\Delta}(Q^2) = 1.6 G_{\pi NN}(Q^2)$ can be used to determine the Q^2 behavior of $G_{\pi N\Delta}$ from that of $G_{\pi NN}$. The dashed-dotted line in Fig. 21 shows the resulting curve, which approximates the results well.

In Fig. 22, we show results for $G_{\pi N\Delta}(Q^2)$ and $G_{\pi NN}(Q^2)$ at all values of the quark masses considered in this work. Assuming pion pole dominance we relate the $G_{\pi NN}$ and $G_{\pi N\Delta}$ to G_P and C_6^A respectively using Eq. (47). Taking the functions defined in Eq. (50) for the Q^2-dependence of $G_p(Q^2)$ and $C_6^A(Q^2)$, we write

$$G_{\pi NN}(Q^2) = K_N \frac{Q^2/m_\pi^2 + 1}{(Q^2/m_A^2 + 1)^2 (Q^2/m^2 + 1)} \qquad (53)$$

with a corresponding expression for $G_{\pi N\Delta}(Q^2)$. The only free parameter is an overall constant, K_N, to be fitted to the results. The value of K_N determines $g_{\pi NN}$ and is given in Table III. The fits to the quenched data at the smallest quark mass using Eq. (53) are shown by the dashed lines in Fig. 22. Note that if m were the pion mass, then the pole term would cancel, leaving a dipole Q^2-dependence for these form factors. Allowing $m \neq m_\pi$ and adjusting the overall strength, we can obtain a reasonable description of the Q^2- dependence of $G_{\pi NN}$ and $G_{\pi N\Delta}$. Since lattice results for these form factors do not increase at low values of Q^2 as fast as expected by PCAC, we obtain a smaller value at $Q^2 = 0$. The values of $g_{\pi NN} = G_{\pi NN}(0)$ and $g_{\pi N\Delta} = G_{\pi N\Delta}(0)$ extracted using Eq. (53), when the fit yields $\chi^2/\text{d.o.f.} \lesssim 1.5$, are given in Table III. If one uses the relation $G_{\pi NN}(Q^2) = (m_N/f_\pi) G_A(Q^2)$ as the GTR would suggest, then the extrapolated value at the lightest pion mass would be $g_{\pi NN} = 11.8 \pm 0.3$ in the quenched theory closer to the experimental value of $13.21^{+0.11}_{-0.05}$ [45]. Therefore the different low Q^2 dependence observed in the lattice results compared to what is usually assumed, is responsible for the lower values of $g_{\pi NN}$ and $g_{\pi N\Delta}$ extracted from these fits.

VI. SUMMARY AND CONCLUSIONS

We have presented results for the nucleon axial-vector form factors $G_A(Q^2)$ and $G_p(Q^2)$ as well as for the corresponding N to Δ axial transition form factors $C_5^A(Q^2)$ and $C_6^A(Q^2)$. The πNN and $\pi N\Delta$ form factors $G_{\pi NN}(Q^2)$ and $G_{\pi N\Delta}(Q^2)$ are also evaluated. Using ratios that show very weak quark mass dependence and are therefore expected to have the same value in the physical limit, we reach a number of phenomenologically important conclusions. One of the main conclusions is that $G_{\pi NN}$ and $G_{\pi N\Delta}$ have the same Q^2 dependence yielding a ratio of $G_{\pi N\Delta}(Q^2)/G_{\pi NN}(Q^2) = 1.60(2)$ in good agreement with what is expected phenomenologically. Similarly the ratio $2C_5^A(Q^2)/G_A(Q^2) = 1.63(1)$ is also independent of Q^2. Equality of these two ratios implies the Goldberger-Treiman relations. The ratio $8C_6^A(Q^2)/G_p(Q^2)$ on the other hand is larger by about 6%. The popular pion pole dominance hypothesis is examined using our lattice results. We find that in the quenched theory the ratios of $G_p(Q^2)/G_A(Q^2)$ and $C_6^A(Q^2)/C_5^A(Q^2)$ require a larger pole mass m than the corresponding pion mass in order to get a good description at low values of Q^2. On the other hand, these ratios in the hybrid approach are well described with $m \sim m_\pi$. However the overall strength differs from what is predicted using the Goldberger-Treiman relations.

We also studied the Q^2-dependence of the form factors separately. Comparing quenched and unquenched results at pion mass of about 350 MeV, we observe large unquenching effects on the low Q^2-dependence of the four form factors, $G_A(Q^2)$, $G_P(Q^2)$, $C_5^A(Q^2)$, and $C_6^A(Q^2)$. This confirms the expectation that pion cloud effects are expected to be large at low Q^2. We find that the Q^2-dependence of the form factors G_A and C_5^A is well described by a dipole of the

form $c_0/(1 + Q^2/m_A^2)^2$. For the pion masses used in this work we find that $m_A \gtrsim 1.5$ GeV as compared to 1.1 GeV used to describe the Q^2 of experimental data for G_A. An exponential Ansatz of the form $\tilde{c}_0 \exp(-Q^2/\tilde{m}_A^2)$ also provides a good description of the Q^2-dependence. In agreement with a recent lattice evaluation of the nucleon axial charge g_A [23], we find that g_A increases when using unquenched configurations on a large volume and pion mass of about 350 MeV becoming consistent with experiment. A different low Q^2-dependence is observed for both quenched and unquenched results in the case of $G_{\pi NN}(Q^2)$ and $G_{\pi N\Delta}(Q^2)$. Instead of the dipole form expected from the Goldberger-Treiman relations of Eq. (14) one finds that $G_{\pi NN}$ and $G_{\pi N\Delta}$, in the limit $Q^2 \to 0$, increase less rapidly. As a result of this, the values that we extract for the strong coupling constants $g_{\pi NN} = \lim_{Q^2\to 0} G_{\pi NN}(Q^2)$ and $g_{\pi N\Delta} = \lim_{Q^2\to 0} G_{\pi N\Delta}(0)$ are smaller than those extracted from experiment. One ingredient that is needed for the determination of these form factors is the renormalized quark mass. In this work, we use the axial Ward identity to determine it. On the lattice, the axial Ward identity has $\mathcal{O}(a)$ corrections in the case of Wilson fermions, which can become important, in particular, as we approach the physical limit. In the case of domain wall fermions, the axial Ward identity is only exact in the limit of large fifth dimension with corrections due to the residual mass, which again become more important in the chiral limit. The renormalized quark mass, however, affects the overall strength of these form factors and therefore it cannot explain the different Q^2-dependence. To investigate this issue further one would like to use lighter quark masses on a finer lattice. This will become feasible in the near future as such dynamical simulations are under way.

ACKNOWLEDGMENTS

We would like to thank B. Orth, Th. Lippert, and K. Schilling [30] as well as C. Urbach, K. Jansen, A. Shindler, and U. Wenger [31] and the MILC collaboration for providing the unquenched configurations used in this work, as well as the LHP collaboration for providing forward propagators [37]. A. T. would like to acknowledge support by the University of Cyprus and the program ''Pythagoras'' of the Greek Ministry of Education. The computations for this work were partly carried out on the IBM machine at NIC, Julich, Germany. This work is supported in part by the EU Integrated Infrastructure Initiative Hadron Physics (I3HP) under contract RII3-CT-2004-506078 and by the U.S. Department of Energy (D.O.E.) Office of Nuclear Physics under contract DE-FG02-94ER40818. This research used resources of the National Energy Research Scientific Computing Center, which is supported by the Office of Science of the U.S. Department of Energy under Contract No. DE-AC03-76SF00098 and the MIT Blue Gene computer, supported by the DOE under Grant No. DE-FG02-05ER25681.

APPENDIX

TABLE V. The first column gives the Q^2 in GeV^2, the second G_A/Z_A, the third G_p/Z_A, and the fourth $G_{\pi NN}$ for quenched Wilson fermions. The errors quoted are jackknife errors.

Nucleon elastic:Quenched Wilson fermions			
Q^2 (GeV^2)	G_A/Z_A	G_p/Z_A	$G_{\pi NN}$
$m_\pi = 0.563(4)$ (GeV)			
0.0	1.332(17)		
0.17	1.193(13)	12.117(188)	9.645(232)
0.34	1.077(16)	8.456(169)	9.296(139)
0.49	0.977(15)	6.227(153)	8.804(202)
0.64	0.893(15)	5.102(157)	8.294(240)
0.79	0.825(18)	4.123(95)	7.799(254)
0.93	0.752(18)	3.277(111)	7.318(286)
1.19	0.662(25)	2.502(117)	6.352(374)
1.32	0.589(27)	2.037(102)	5.738(380)
1.44	0.557(31)	1.885(114)	5.384(456)
1.56	0.502(32)	1.563(106)	4.910(475)
1.68	0.421(38)	1.220(141)	3.780(565)
1.79	0.451(47)	1.307(147)	4.177(590)
1.90	0.371(40)	1.001(119)	3.374(497)
2.12	0.337(86)	0.951(274)	2.437(881)
$m_\pi = 0.490(4)$ (GeV)			
0.0	1.325(15)		
0.17	1.183(15)	12.432(321)	9.109(190)
0.33	1.065(21)	8.352(147)	8.845(166)
0.49	0.961(23)	5.964(169)	8.419(243)
0.64	0.879(20)	4.914(166)	7.850(247)
0.78	0.811(15)	3.902(116)	7.457(262)
0.91	0.738(22)	3.044(109)	7.065(318)
1.17	0.654(28)	2.317(124)	6.183(421)
1.29	0.577(30)	1.874(108)	5.534(428)
1.41	0.546(33)	1.750(119)	5.037(487)
1.53	0.489(36)	1.426(110)	4.677(518)
1.64	0.409(42)	1.094(147)	3.644(657)
1.75	0.451(55)	1.234(161)	4.055(651)
1.86	0.363(45)	0.917(126)	3.246(537)
2.07	0.323(93)	0.853(282)	2.033(903)
$m_\pi = 0.411(4)$ (GeV)			
0.0	1.319(19)		
0.17	1.177(19)	12.824(345)	8.619(182)
0.33	1.054(22)	8.225(202)	8.417(232)
0.48	0.947(19)	5.649(185)	8.085(277)
0.63	0.867(28)	4.700(199)	7.380(309)
0.76	0.798(21)	3.650(117)	7.102(301)
0.90	0.723(27)	2.762(120)	6.886(393)
1.14	0.647(36)	2.084(142)	6.167(535)
1.26	0.566(35)	1.685(117)	5.405(550)
1.38	0.538(40)	1.601(128)	4.601(541)
1.49	0.474(41)	1.269(118)	4.434(589)
1.60	0.394(47)	0.938(164)	3.549(854)
1.70	0.453(67)	1.148(187)	4.009(777)
1.81	0.353(52)	0.817(142)	3.217(633)
2.00	0.324(115)	0.778(322)	1.578(986)

TABLE VI. The first column gives the Q^2 in GeV^2, the second G_A/Z_A, the third G_p/Z_A, and the fourth $G_{\pi NN}$ for dynamical Wilson fermions. The errors quoted are jackknife errors.

Nucleon elastic: $N_F = 2$ Wilson fermions			
Q^2 (GeV^2)	G_A/Z_A	G_p/Z_A	$G_{\pi NN}$
$m_\pi = 0.691(8)$ (GeV)			
0.0	1.382(11)		
0.43	1.105(16)	8.976(298)	9.367(228)
0.82	0.893(16)	5.115(170)	8.361(278)
1.19	0.735(22)	3.075(172)	7.696(361)
1.53	0.658(36)	2.575(193)	6.621(516)
1.86	0.592(44)	2.033(190)	5.980(552)
2.17	0.484(45)	1.325(159)	5.460(617)
2.75	0.356(91)	1.108(322)	2.441(788)
3.03	0.290(74)	0.678(212)	3.081(853)
$m_\pi = 0.509(8)$ (GeV)			
0.0	1.270(27)		
0.42	0.982(21)	7.229(388)	8.505(350)
0.81	0.809(24)	3.914(221)	7.827(331)
1.16	0.657(32)	1.983(225)	7.913(517)
1.49	0.502(50)	0.668(218)	7.689(1.057)
1.79	0.457(43)	0.663(151)	7.005(860)
2.09	0.377(72)	0.300(161)	7.416(1.691)
2.63	0.216(74)	0.702(143)	4.551(1.841)
2.88	0.104(60)	−0.025(84)	3.298(1.897)
3.12	0.028(25)	0.226(54)	0.651(0.442)
$m_\pi = 0.384(8)$ (GeV)			
0.0	1.175(33)		
0.42	0.990(25)	5.418(370)	7.812(391)
0.78	0.835(32)	3.395(244)	6.454(366)
1.11	0.786(49)	2.269(221)	5.166(549)
1.41	0.611(50)	1.270(220)	5.673(689)
1.68	0.632(98)	1.361(223)	4.867(1.017)
1.95	0.476(77)	0.979(177)	2.058(734)
2.43	0.092(527)	0.241(1.377)	0.638(5.365)

TABLE VII. The first column gives the Q^2 in GeV^2, the second C_5^A/Z_A, the third C_6^A/Z_A, and the fourth $G_{\pi N\Delta}$ for quenched Wilson fermions. The errors quoted are jackknife errors.

N to Δ: Quenched Wilson fermions			
Q^2 (GeV^2)	C_5^A/Z_A	C_6^A/Z_A	$G_{\pi N\Delta}$
$m_\pi = 0.563(4)$ (GeV)			
0.16	1.016(14)	2.675(81)	15.613(356)
0.35	0.902(8)	1.778(52)	15.207(298)
0.53	0.803(15)	1.269(45)	14.441(361)
0.70	0.712(14)	1.012(38)	12.795(501)
0.87	0.635(17)	0.774(26)	11.882(415)
1.03	0.571(18)	0.607(26)	11.203(442)
1.34	0.465(21)	0.418(24)	9.610(538)
1.48	0.414(23)	0.348(23)	8.440(515)
1.63	0.371(25)	0.305(26)	7.318(681)
1.77	0.330(25)	0.247(23)	6.895(639)
1.90	0.295(31)	0.204(26)	5.744(764)
2.03	0.273(32)	0.188(25)	6.216(856)
2.16	0.230(28)	0.145(20)	5.106(669)
2.42	0.172(48)	0.116(39)	3.603(1.527)
$m_\pi = 0.490(4)$ (GeV)			
0.16	0.999(14)	2.741(105)	14.396(351)
0.35	0.885(16)	1.741(52)	14.343(325)
0.53	0.787(16)	1.202(46)	13.758(354)
0.70	0.691(18)	0.950(44)	11.918(535)
0.87	0.616(19)	0.712(30)	11.200(441)
1.03	0.553(22)	0.552(26)	10.717(456)
1.34	0.450(26)	0.377(25)	9.412(592)
1.48	0.401(26)	0.313(24)	8.129(572)
1.62	0.357(28)	0.274(27)	6.807(751)
1.76	0.315(29)	0.220(24)	6.563(708)
1.90	0.288(36)	0.183(27)	5.584(883)
2.03	0.262(36)	0.169(26)	6.176(966)
2.15	0.219(31)	0.129(21)	5.015(735)
2.40	0.150(48)	0.092(37)	3.466(1.749)
$m_\pi = 0.411(4)$ (GeV)			
0.15	0.975(19)	2.804(129)	12.928(392)
0.34	0.864(16)	1.688(71)	13.263(315)
0.53	0.769(19)	1.114(58)	13.023(474)
0.71	0.668(19)	0.876(52)	10.784(719)
0.87	0.593(23)	0.634(34)	10.453(479)
1.04	0.536(25)	0.488(27)	10.225(563)
1.34	0.438(30)	0.333(28)	9.496(718)
1.49	0.391(31)	0.272(25)	7.978(684)
1.63	0.347(32)	0.240(30)	6.303(901)
1.77	0.303(34)	0.190(26)	6.269(848)
1.90	0.284(44)	0.157(29)	5.555(1.089)
2.03	0.250(44)	0.150(28)	6.346(1.179)
2.15	0.211(37)	0.113(22)	5.127(870)
2.40	0.121(50)	0.065(37)	3.425(2.354)

TABLE VIII. The first column gives the Q^2 in GeV^2, the second C_5^A/Z_A, the third C_6^A/Z_A, and the fourth $G_{\pi N\Delta}$ for dynamical Wilson fermions. The errors quoted are jackknife errors.

N to Δ: $N_F = 2$ Wilson fermions			
Q^2 (GeV^2)	C_5^A/Z_A	C_6^A/Z_A	$G_{\pi N\Delta}$
$m_\pi = 0.691(8)$ (GeV)			
0.449	0.956(16)	2.022(93)	16.082(457)
0.882	0.765(19)	1.080(57)	13.653(480)
1.286	0.605(23)	0.586(41)	12.253(656)
1.666	0.500(34)	0.457(48)	10.671(945)
2.025	0.444(38)	0.371(39)	8.990(863)
2.367	0.361(37)	0.240(32)	8.210(1.029)
3.008	0.229(63)	0.162(49)	4.431(1.341)
3.310	0.161(45)	0.083(37)	4.961(1.391)
$m_\pi = 0.509(8)$ (GeV)			
0.441	0.845(23)	1.517(111)	13.761(622)
0.895	0.673(23)	0.744(55)	11.611(668)
1.311	0.552(29)	0.380(46)	9.955(1.049)
1.697	0.502(55)	0.240(56)	8.599(1.500)
2.059	0.382(38)	0.161(28)	7.389(1.124)
2.401	0.305(65)	0.083(30)	7.213(1.880)
3.035	0.144(62)	0.039(25)	3.656(2.079)
$m_\pi = 0.384(8)$ (GeV)			
0.443	0.837(28)	1.335(96)	11.302(722)
0.891	0.700(25)	0.583(46)	11.997(792)
1.293	0.620(34)	0.381(35)	8.956(1.0358)
1.661	0.530(38)	0.256(29)	9.168(1.482)
2.002	0.452(63)	0.203(30)	5.966(1.504)
2.322	0.342(48	0.136(22)	2.054(1.086)
3.183	0.102(23)	0.030(9)	0.950(6.900)

TABLE IX. The first column gives the Q^2 in GeV^2, the second C_5^A/Z_A, the third C_6^A/Z_A, and the fourth $G_{\pi N\Delta}$ in the hybrid approach. The errors quoted are jackknife errors. Note that we include the errors on Q^2 for the smaller pion mass since the uncertainty on the lowest Q^2 value is about 40%.

N to Δ: Hybrid action			
Q^2 (GeV^2)	C_5^A/Z_A	C_6^A/Z_A	$G_{\pi N\Delta}$
$m_\pi = 0.594(1)$ (GeV)			
0.216	0.689(13)	2.131(92)	16.602(449)
0.484	0.642(16)	1.326(60)	16.359(563)
0.739	0.578(18)	0.944(57)	14.796(808)
0.983	0.490(19)	0.614(43)	13.944(1.049)
1.217	0.444(22)	0.477(32)	12.911(1.094)
1.442	0.392(26)	0.377(31)	11.178(1.315)
1.871	0.317(46)	0.244(45)	10.628(2.508)
2.075	0.261(39)	0.180(32)	9.296(2.253)
2.273	0.220(39)	0.132(29)	9.768(3.075)
2.466	0.201(50)	0.118(32)	10.702(3.698)
2.654	0.132(73)	0.115(63)	4.125(4.734)
2.838	0.101(90)	0.041(47)	11.147(10.192)
$m_\pi = 0.498(3)$ (GeV)			
0.198	0.683(33)	2.398(186)	15.404(608)
0.475	0.621(27)	1.212(77)	15.823(667)
0.736	0.540(32)	0.809(75)	15.325(896)
0.985	0.548(42)	0.686(76)	13.718(1.466)
1.222	0.446(34)	0.445(44)	12.040(1.226)
1.449	0.385(38)	0.332(40)	10.760(1.523)
1.879	0.296(53)	0.191(42)	10.334(3.357)
2.083	0.284(67)	0.182(47)	4.914(2.902)
2.280	0.325(116)	0.190(70)	2.688(5.406)
2.472	0.208(106)	0.101(59)	2.967(5.431)
2.658	0.125(134)	0.102(99)	
$m_\pi = 0.353(2)$ (GeV)			
0.038(16)	0.532(41)	3.443(197)	11.266(513)
0.190(14)	0.603(28)	2.269(129)	12.930(616)
0.337(8)	0.612(25)	1.624(109)	12.625(709)
0.479(9)	0.589(26)	1.237(82)	13.112(957)
0.617(8)	0.557(26)	0.939(59)	12.031(899)
0.750(10)	0.533(28)	0.758(56)	10.377(957)
1.0059(11)	0.478(37)	0.511(55)	9.666(1.377)
1.128(16)	0.459(38)	0.466(47)	7.578(1.302)
1.248(10)	0.420(39)	0.383(44)	8.318(1.659)
1.365(23)	0.410(44)	0.339(44)	8.292(1.625)
1.479(5)	0.406(72)	0.351(72)	5.011(3.019)
1.591(18)	0.380(61)	0.249(47)	10.413(2.627)
1.701(35)	0.376(71)	0.246(52)	7.491(2.716)
1.914(6)	0.247(81)	0.155(56)	

[1] H.-Y. Gao *et al.* (BLAST Collaboration), in *Intersections of Particle and Nuclear Physics*, edited by Tony M. Liss, AIP Conf. Proc. No. 870 (AIP, New York, 2006); H. Gao, Int. J. Mod. Phys. E **12**, 1 (2003); **12**, 567(E) (2003); Ch. E. Hyde-Wright and K. de Jager, Annu. Rev. Nucl. Part. Sci. **54**, 217 (2004).

[2] C. F. Perdrisat, V. Punjabi, and M. Vanderhaeghen, arXiv:hep-ph/0612014; J. Arrington, C. D. Roberts, and J. M. Zanotti, J. Phys. G **34**, S23 (2007).

[3] N. F. Sparveris *et al.*, Phys. Rev. Lett. **94**, 022003 (2005); C. Mertz *et al.*, Phys. Rev. Lett. **86**, 2963 (2001).

[4] K. Joo *et al.*, Phys. Rev. Lett. **88**, 122001 (2002).

[5] V. Pascalutsa and M. Vanderhaeghen, Phys. Rev. Lett. **95**, 232001 (2005); Phys. Rep. **437**, 125 (2007).
[6] T. A. Gail and Th. R. Hemmert, Eur. Phys. J. A **28**, 91 (2006).
[7] C. Alexandrou *et al.*, Phys. Rev. D **69**, 114506 (2004).
[8] C. Alexandrou *et al.*, Phys. Rev. Lett. **94**, 021601 (2005).
[9] C. Alexandrou *et al.*, Nucl. Phys. B, Proc. Suppl. **129**, 302 (2004); C. Alexadrou, Nucl. Phys. B, Proc. Suppl. **128**, 1 (2004); C. Alexandrou *et al.*, Nucl. Phys. B, Proc. Suppl. **140**, 293 (2005); Proc. Sci., LAT2005 (2006) 091.
[10] A. L. Ahrens *et al.*, Phys. Lett. B **202**, 284 (1988).
[11] V. Bernard, N. Kaiser, and U.-G. Meissner, Phys. Rev. Lett. **69**, 1877 (1992).
[12] S. Choi *et al.*, Phys. Rev. Lett. **71**, 3927 (1993).
[13] T. Gorringe and H. W. Fearing, Rev. Mod. Phys. **76**, 31 (2004).
[14] V. Bernard, L. Elouadrhiri, and U.-G. Meissner, J. Phys. G **28**, R1 (2002).
[15] M. R. Schindler, T. Fuchs, J. Gegelia, and S. Scherer, Phys. Rev. C **75**, 025202 (2007).
[16] S. L. Adler, Ann. Phys. (N.Y.) **50**, 189 (1968); Phys. Rev. D **12**, 2644 (1975).
[17] N. C. Mukhopadhyay, M. J. Ramsey-Musolf, St. J. Pollock, J. Liu, and H.-W. Hammer, Nucl. Phys. **A633**, 481 (1998).
[18] S. J. Barish *et al.*, Phys. Rev. D **19**, 2521 (1979).
[19] S. P. Wells, PAVI 2002, Mainz, Germany, 2002 (unpublished); (private communication).
[20] D. Dolgov *et al.* (LHPC Collaboration and TXL Collaboration), Phys. Rev. D **66**, 034506 (2002).
[21] M. Göckeler *et al.* (QCDSF Collaboration), Phys. Rev. D **71**, 034508 (2005); T. Bakeyer *et al.* (QCDSF-UKQCD Collaboration), Nucl. Phys. B, Proc. Suppl. **128**, 82 (2004).
[22] C. Alexandrou, G. Koutsou, J. W. Negele, and A. Tsapalis, Phys. Rev. D **74**, 034508 (2006).
[23] R. G. Edwards *et al.* (LHPC Collaboration), Phys. Rev. Lett. **96**, 052001 (2006).
[24] A. Ali Khan *et al.*, Phys. Rev. D **74**, 094508 (2006).
[25] T. Blum *et al.*, Phys. Rev. D **68**, 054509 (2003).
[26] R. G. Edwards *et al.*, Proc. Sci., LAT2006 (2007) 195.
[27] Ph. Hägler *et al.*, arXiv:0705.4295.
[28] C. Alexandrou, Th. Leontiou, J. W. Negele, and A. Tsapalis, Phys. Rev. Lett. **98**, 052003 (2007); Proc. Sci. LAT2006 (2007) 115 [arXiv:hep-lat/0610107].
[29] K. F. Liu, S. J. Dong, T. Draper, and W. Wilcox, Phys. Rev. Lett. **74**, 2172 (1995).
[30] B. Orth, Th. Lippert, and K. Schilling ($T\chi L$ Collaboration), Phys. Rev. D **72**, 014503 (2005); Th. Lippert *et al.*, Nucl. Phys. B, Proc. Suppl. **60A**, 311 (1998).
[31] C. Urbach *et al.*, Comput. Phys. Commun. **174**, 87 (2006).
[32] K. Orginos, D. Toussaint, and R. L. Sugar, Phys. Rev. D **60**, 054503 (1999).
[33] C. Alexandrou, in *Shapes of Hadrons*, edited by C. N. Papanicolas and A. M. Bernstein, AIP Conf. Proc. No. 904 (AIP, New York, 1994); arXiv:hep-lat/0611008.
[34] C. H. Llewellyn Smith, Phys. Rep. **3C**, 261 (1972).
[35] V. Furman and Y. Shamir, Nucl. Phys. **B439**, 54 (1995).
[36] T. Blum *et al.*, Phys. Rev. D **69**, 074502 (2004).
[37] D. Renner *et al.* (LHP Collaboration), Nucl. Phys. B, Proc. Suppl. **140**, 255 (2005).
[38] C. Aubin *et al.*, Phys. Rev. D **70**, 094505 (2004).
[39] C. Alexandrou *et al.*, Nucl. Phys. **B414**, 815 (1994).
[40] A. Hasenfratz and F. Knechtli, Phys. Rev. D **64**, 034504 (2001).
[41] Ph. Hägler *et al.*, Phys. Rev. D **68**, 034505 (2003).
[42] V. Giménez, L. Guisti, F. Rapuano, and M. Talevi, Nucl. Phys. **B531**, 429 (1998).
[43] D. Bećirević *et al.*, Nucl. Phys. **B734**, 138 (2006).
[44] T. Kitagaki *et al.*, Phys. Rev. D **42**, 1331 (1990).
[45] H. C. Schröder *et al.*, Eur. Phys. J. C **21**, 473 (2001).